Study of Fragmentation Dynamics of Polyatomic Molecules

A THESIS

submitted for the Award of Ph. D. degree of

MOHANLAL SUKHADIA UNIVERSITY

in the

Faculty of Science

by

Rajesh Kumar Kushawaha

Under the Supervision of

Bhas Bapat, Associate Professor
Physical Research Laboratory, Ahmedabad

DEPARTMENT OF PHYSICS

FACULTY OF SCIENCE

MOHANLAL SUKHADIA UNIVERSITY

UDAIPUR

Year of submission 2009

माई – बाऊजी
को
अर्पित

Contents

Certificate

I feel great pleasure in certifying that the thesis entitled "Study of Fragmentation Dynamics of Polyatomic Molecules" embodies a record of the results of investigations carried out by Rajesh Kumar Kushawaha under my guidance. I am satisfied with the analysis of data, interpretation of results and conclusions drawn.

He has completed the residential requirement as per rules.

I recommend the submission of thesis.

Bhas Bapat
Associate Professor
Physical Research Laboratory
Ahmedabad

Date:
10 October 2009

Declaration

I hereby declare that the work incorporated in the present thesis entitled "Study of Fragmentation Dynamics of Polyatomic Molecules" is my own work and is original. This work (in part or in full) has not been submitted to any University for the award of a Degree or a Diploma.

Rajesh Kumar Kushawaha

Abstract

This dissertation concerns the study of fragmentation dynamics of polyatomic molecular ions created by the impact of high energy electrons on neutral molecules. We pay particular attention to the rare process of *associative fragmentation*, i.e. the formation of a bond between atoms that are separated in the neutral molecule, but get associated during the evolution of the neutral molecule into an unstable molecular ion. Investigation of migration of atoms and bond formation between the atoms in the molecular ion during fragmentation using the multi-ion coincidence momentum imaging technique is the focus of the thesis.

Association, as described above, can occur in molecules with at least three atoms. To begin, atom-atom association in linear and bent triatomic molecules like CO_2, CS_2 and H_2O are studied from the view point of deciphering the role of the geometry of the target molecule in formation of various associative ions. The formation of H_2^+ and S_2^+ ions from the dissociative ionization of H_2O and CS_2 molecules has been observed. Formation of these associative ions suggests that geometrical deformation of molecular ion probably activates the association reaction.

This idea is extended to polyatomic molecules. We have initially chosen the symmetric tetrahedral CH_4 molecule for investigation of intra-molecular association between hydrogen atoms. We have observed the formation of H_2^+ ion from singly and doubly ionized CH_4 molecule. In this molecule,

all H atoms are equivalent and the possibility of association between any two H atom is the same. The association reaction would be altered if we replaced any one H atom by another atom, especially by a highly electronegative atom or radical. Hence, we have investigated the *atom substitution effect* on the H–H association reaction in CH_4 molecule. This is done by changing over to molecules such as CH_3Cl and CH_3OH and observing the association of H atoms. In addition to the formation of H_2^+, H_3^+ is found to arise from dissociative ionization of CH_3Cl and CH_3OH, which was not observed in CH_4. In fact, the presence of the –Cl radical enhances triple association (H_3^+) even more than pair association (H_2^+). This implies that deviation from tetrahedral symmetry in CH_3Cl^{2+} is large and brings the three H atoms very close to each other. Similar distortion mechanism appears to be present in CH_3OH, but its effect is more favourable for pair association, than triple association.

The role of chemical group (methyl and hydroxyl groups) in bond association is investigated in the CH_3OH molecule. To distinguish between the H atom of hydroxyl group or methyl group, we have used the *isotope tagging method*. Substituting the H atoms in methyl group by D atoms (i.e. performing the experiment with CD_3OH instead of CH_3OH), we are able to identify whether a certain reaction channel involves the hydroxyl or the methyl group. This enables investigation of *site-specific atom-atom association*. We found that the formation probability of H_3^+ and H_2^+ from methyl group alone is five times more than the formation of same ions from both group of H atom migration and association.

We have looked into *multi-atom migration and bond association* in various polyatomic hydrocarbon molecules. In C_2H_5OD, we have observed the formation of ODH_2^+ ion, which is evidence of two H atom migration and association. The effect of small geometrical differences between two structurally very similar molecules such as CH_3COCH_3 and CH_3SOCH_3 and the possibility of more than two atom migration has also been looked into. We have found evidence of three atom migration and formation of OH_3^+ ion from fragmenting CH_3SOCH_3 dication, but the same fragment is not observed from CH_3COCH_3. We attribute this to the small geometric difference in the two molecules. We have done a momentum map analysis for investigation of break-up pattern of the precursor and formation of this ion. We have found that the OH_3^+ ion is ejected in concerted three-body break-up process.

The last part of the thesis concerns *modelling or estimation of some geometrical parameters of the precursor molecular ion*. All precursors in which the associative ions originate have to be in a deformed geometrical states, when compared to the ground state geometry of the parent neutral, so that associative reactions may be initiated. We have mapped the geometry of molecular ions which eject associative ions in three-body break-ups. Mapping the geometry of these ions using kinematically complete experimental data can provide plenty of information that may be related to the potential energy surfaces responsible for the observed fragmentation channels, and can help in exploring the association reaction in depth. Using the momentum imaging technique we have successfully mapped the geometry of CH_3Cl^{2+} and found that the geometry of this ion is planar rather than deformed tetrahedral. Using a simple model, we relate the kinetic energy release and momentum distributions of the fragments of CH_3Cl^{2+} in a three body break-up to some of the initial geometric parameters of the fragmenting molecular ion. Further, the trajectories of the fragments in triple fragmentation of a triply ionized molecular ion (CO_2^{3+}) are simulated and a relation is obtained between the observed vector momenta of the fragments and the bond angle of the molecular ion.

In summary, we have explored various aspects of associative reactions in fragmentation dynamics of polyatomic molecular ion using momentum imaging technique. The association reaction may depend on various factors such as the perturbation, geometry of molecule, electronegative sites in molecule, etc. Our comparative study of associative reactions in various molecules indicates that the deformed geometry of precursor ion play a key role for enhancing the associative ion formation. Further, we have found some signatures of the role of functional groups in a molecule in the kinetic energy distributions of the associative ions. We have been able to show that the momentum maps offer a way of estimating the geometry of the precursor molecular ion under certain conditions, namely when a three-body break-up of a doubly or triply charged precursor ion occurs. In case where there is only one neutral fragment, its kinetic energy can be determined from the momentum balance in the reaction, thus enabling an analysis of the kinetic energy release in the reaction. Modelling of the trajectories of fragments under Coulomb repulsion and comparison of the trajectories with the observed fragment momenta under simple models and assumptions has enabled us to estimate some of the geometrical parameters of the precursor molecular ions.

Chapter 1

Introduction

1.1 An overview

An atom or a molecule is a quantum mechanical bound state system in which the electrons and the nuclei are dynamically arranged in such a way that the system is stable. The curiosity to know how electrons and nucleus are arranged in the atom or molecules was addressed in the first decade of 20th century. The first scattering experiment to understand the structure of atoms was done by Rutherford in 1911 [Rut09]. This breakthrough experiment reveals that the atom consists of a positively charged heavy nucleus with negatively charged electrons arranged around it.

The true beginning of atomic and molecular physics is marked by the discovery of spectral lines. The spectrum lines analysis of atoms was attempted by Bohr [Boh13]. The study of spectral line led to the birth of quantum mechanics. Quantum mechanics explains many issues related to atom and molecules. Some of the predictions of quantum mechanics are experimentally tested. For example, the prediction of discrete energy levels in an atom or molecule have been verified via measurement of spectral lines. The information about the electron and nuclear configuration in bound state system may be obtained from the absorption or emission spectra which is generated when the electromagnetic radiation interacts with them. Various properties of atoms or molecules are determined from the wavelength, intensity, line-width etc of spectral lines. For example the wavelength measurements of spectral lines allow the determination of energy levels of atom or molecules. The intensity of spectrum line measures how strongly two levels of molecular transitions are populated and coupled. Several spectroscopic techniques have been developed to investigate the issues related to electron-electron and electron-nucleus interactions. For example the hyperfine structure measurement of spectrum lines yields the information about the interaction between the nuclei and electron cloud.

A different class of properties of atoms and molecules can be obtained by collision experiments. Such experiments involve collisions between the projectile such as electron, ion or photon and an atomic or molecular system. During the collision, several processes such as elastic or inelastic scattering, dissociation, ionization etc. can occur. The probability of a particular process is measured by specifying the quantity known as cross-section. For a certain type of event in a given collision, the cross-section is defined as the ratio of the number of event of this type per unit time and per unit scatterer, to the flux of the incident particles with respect to the targets. The nature of this quantity depend on the energy of projectile and targets. This quantity can give many kinds of information about the atomic and molecular system, for example the strength of electron–electron and electron–nucleus interaction in bound state system can be obtained by collision experiment. The other example is the global property of an atom or molecule such as the charge density, that can be inferred from the cross-sections for high energy electron scattering [Shi99]. The knowledge of electron–atom or molecular collision cross-sections is very important in various areas such as astrophysics, plasma physics, upper atmospheric process and radiation physics. The study of electron–atom or molecular collision has also been strongly motivated by the need of data for testing and developing suitable theories of the scattering and collision processes, and for providing a tool for obtaining details information on the structure of targets atoms or molecules [Wei73, Fur73].

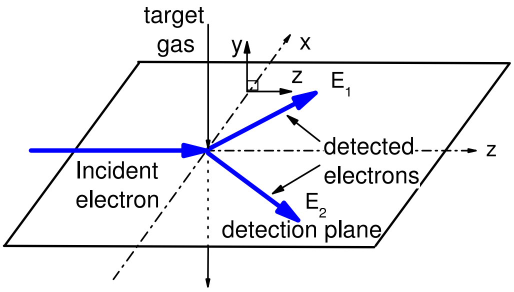

Figure 1.1: The (e,2e) experiment. An incident electron of sufficient energy collides with a target. Both outgoing electrons are detected in coincidence using energy and angle sensitive analyzers.

Although the static properties of atoms and molecules have been studied to a large extent using a variety of spectroscopic techniques and also understood by quantum mechanics, the dynamical properties of such many-body systems are still a major challenge for theory and experiment. The parameter which characterize the atomic and molecular many-particle reactions is known as the fully differential cross-sections (FDCS). In the ionization process, the cross-section depends on the various intrinsic reaction parameter such as the momenta, spins and internal excitation of all reaction products. FDCS is the kinematically-complete description of ionization and provides the most sensitive test of the theory of this process. For study the dynamic properties of atoms or molecule, various experimental attempts have been made. The FDCS have been measured experimentally and investigated theoretically for electron impact single ionization (so called (e,2e)-experiments). An (e,2e) experiment is the measurement of an electron impact ionization process where both the outgoing electrons are detected in coincidence. The schematic view of (e,2e) experiment is shown in Figure 1.1. It is a measurement almost at the limit of what is quantum mechanically knowable and its description presents a substantial challenge to theory. (e,2e) experiments yields complete information about the single ionization process. The results of (e,2e) are explained theoretically by many groups [McC91, Cop94, Lah91]. Complete differential cross sections for double ionization of atomic target (such as He) have been reported by many experimental group [Lah91, Sch93, Hue94, Daw95]. The (e,2e) experiment on a molecular target can also use to probe the molecular wave function.

The attempt for probing the molecular wave function of simple diatomic molecules such as H_2 and D_2 using this technique is reported [Dey75]. This attempt is based on the measurement of (e,2e) angular distribution. Also, the (e,2e) experiment has own limitations, for example the the solid angle of electron acceptance by the analyser is small, typically less than 10^{-3} of 4π. In a two or three-electron coincidence experiment the total coincidence efficiency is thus extremely small (10^{-8}). This explains why, so far, systematic investigations of FDCS could be performed only for a few many-particle reactions.

The investigation about the processes occurring in molecules under perturbation is more difficult than the atoms. As we know that in case of atomic targets in collision experiment, one or more electron and one recoil nucleus are formed on the other hand, even for the simplest molecule, a diatomic molecule, one or more electron and up to two fragments (nucleus) may be formed. Increase of the response channels in molecules (due to larger number of degrees of freedom) makes interpretation difficult. For the diatomic molecule case, the traditional (e,2e) type of experiment can be modified with some success, but in a polyatomic molecule, many electrons and many atomic or molecular fragments may be formed. The kinematic information about each fragments ejected from the fragmenting polyatomic molecular ion is difficult to measure by traditional electron spectroscopy techniques.

A relatively new experimental approach, the recoil ion momentum spectrometry technique (RIMS) overcomes many of the above mentioned problems of kinematically complete experiments. Although the RIMS technique was originally developed for atomic collisions [Mos96, Ull97], it could be easily adapted to studying molecular fragmentation. Many variants of the this technique are in use worldwide [Bag04, Par06, Kim06], and we look at the basic principles, which are common to these variants. A technique that deserves special mention is velocity map imaging, which has also become a popular technique in the last decade [Roe02, Rei02].

The recoil ion momentum spectrometer is based on the simultaneous measurement of flight time of ion and position information. A single electric field is used to guide the ion from the birth to the detector. Depending on their initial momentum, ions will have different trajectories. This problem can be inverted, i.e. if the trajectory is known, one can determine the momentum of that ion. In reactions involving molecules, more than one fragment may be ejected from a particular collision event. The detection of these ions in a time-ordered sequence can provide a great deal of information about the event. In particular, complete kinematic information about all fragments can yield in-depth information about dissociation channels and the potential energy surfaces of the molecular ion. From the complete measurement of ions in sequence and its kinematic information, the multiple-differential cross section can be obtained, which is very useful for understanding the process in multi-particle system. The momentum measurement technique is suitable for few body kinematically complete experiment. Most of the earlier kinematically experiments were focused on either atom or diatomic molecule. We have extended this technique to the investigation of polyatomic molecules. Due to increasing number of atoms in molecules, the complexity of the molecular structure make investigations of polyatomic molecules a challenging task. Because of the large number of degrees of freedom for the internal motion of atoms in molecules, the dynamics of all electrons and nuclei are more complex than diatomic molecule. The study of the fragmentation patterns such as stability, branching ratio between the different fragmentation pathways, etc. are important parameters of fragmenting molecular ions. This thesis is based on the measurements related to various parameters of fragmenting molecular ions, using of a recoil ion momentum spectrometer. The details about the various techniques used in this thesis is discussed in chapter 2. The various issues in fragmenting molecular ions are discussed in next section.

1.2 Issues addressed in this work

In this thesis, an attempt has been made to explore the processes that occur in unstable molecular ions. The electron-electron correlations play an important role in the evolution of the molecular state and stability of molecular ion [Gil60, Lev84]. An unstable molecular ion is a Coulombically coupled many-particle quantum system. The dynamics of such a system is still not well known and is a subject of current research. Molecular parameters such as bond length and bond angle may change during the evolution from ground state of the neutral to the dissociative state of the molecular ion. The minimum energy state of system or the stability of molecular ion can be achieved by the geometrical deformation and reorganization of bond within the molecular ion. Further, bond formation between the nearest neighbor atoms may be possible. In certain cases, atom migration and bond formation within the molecular ion may take place. When the unstable polyatomic molecular ion dissociates, the ejected fragments carry the information about the intra-molecular association processes. The detection of various fragments combined with complete kinematic information is extremely useful for studying unstable polyatomic molecular ion.
The central theme is the understanding of factors such as distortion of the geometry of the molecular ion (when compared to the geometry of the neutral molecule), that are responsible for association of atoms during fragmentation. The thesis has evolved along the following points.

1. Atom-atom association in linear and bent triatomic molecules and exploring the role of the geometry of the target molecule in formation of various associative ions.

2. Association in symmetric tetrahedral polyatomic molecule such as CH_4 and exploring the atom substitution effect on the H–H association reaction in CH_4 molecule.

3. Role of chemical groups (methyl and hydroxyl groups) in bond asso-

ciation of molecule in CH_3OH and explore the *site-specific atom-atom association*.

4. Multi-atom migration and bond association in various polyatomic hydrocarbon molecules.
5. Estimation/modelling of the geometrical parameters of the precursor molecular ion during bond association.

1.3 Outline of the thesis

Chapter 1 will provide a brief description of the basic features of dissociative ionization of molecules. The formation of molecular ions, various dissociative channels and attempted to explore the various unresolved issued are discussed in brief.

Chapter 2, 3 describes the experimental setup used for performing the electron-impact molecular dissociation experiments reported in this thesis. The measurement of kinematic parameter may used to extract the properties of molecular ions and its dissociative channels. This chapter also includes the data analysis methodology adopted for determining the momentum components from the raw data. The principle and method of experimental setup, calibration, and method for estimating the geometry of molecular ions are discussed in this chapter.

Chapters 4, 5 and 6 will cover the important findings of the present work. In chapter 4 we have discussed the bond association phenomena in various triatomic molecules such as bent H_2O and linear CO_2 and CS_2 molecule under perturbation. Site specific association, atom substitution effect in association etc are discussed in detail. In chapter 5 we have discussed the possibility of multi atom migration and association. We have proposed that the bent or distorted molecule may induce or influence the multi atom migration. The chapter 6 has covered the mapping of dissociative geometry. Classical trajectory simulation for two- and three-body charge separation has been done to compare the experimentally mapped geometry of molecular ion.

Chapter 7 contains a summary of the thesis, a few suggestions for the continuation of the reported work and new possibilities that have opened up for further studies in this field.

Chapter 2

Experimental Techniques

Probing the processes occurring at the molecular level requires an advanced experimental technique which is capable of detecting or measuring some parameter which is directly related to the processes. In molecular fragmentation, usually, neutral molecules are perturbed by photon or energetic charged particle such as electron and ions. An unstable molecular ion may be formed due to perturbation and usually dissociates into two or many fragments. One of the ways, leading to complete information involves detection of all fragments ejected from the dissociation of molecular ion. Simultaneously, we have to measure the kinematic parameter such as momentum or energy of each fragment. For detecting the ion fragments, the successful and popular technique is the time-of flight technique. Further, for kinematic parameter measurement, techniques such as coincidence technique and ion momentum imaging have been developed. In this chapter, we described the working principle of the ion momentum spectrometry which is used for study the fragmentation dynamics of molecules.

2.1 Principle of an ion momentum spectrometer

In this section, we discuss the principle of the ion momentum spectrometer. The spectrometer is based on the well localized reaction zone and electric fields to guide all charged fragments towards large-area position- and time-sensitive detectors. From the measurement of the time-of-flight and the position of impact for each particle its momentum vector can be determined. Details about the time-of-flight for detection of ion, position sensitive anode technique for detection of position of ion and coincidence technique for detection of ions in time sequence are discussed in separate sections.

2.1.1 Time-of-flight measurement

The time-of-flight mass spectroscopy (TOFMS) is suitable technique for detecting and mass analyzing charged fragments. This technique based on the measurement of the flight time of ion which reaches to a detector while traveling over a known distance in an electric field. The velocity of ion depends on the mass-to-charge ratio. Depending on the mass resolution requirement, different kind of TOF spectrometer such as single field or double field, and reflectron mass spectrometer have been invented [Wil55, Boe82, Cha94, Ber90]. For our study, single field TOF spectrometer have been used. Thus, we will discuss only the principle of single field TOF mass spectrometer. A linear single field TOF spectrometer is shown in Figure 2.1. It is consists of extraction field region, s (pusher and puller plate for ion extraction)

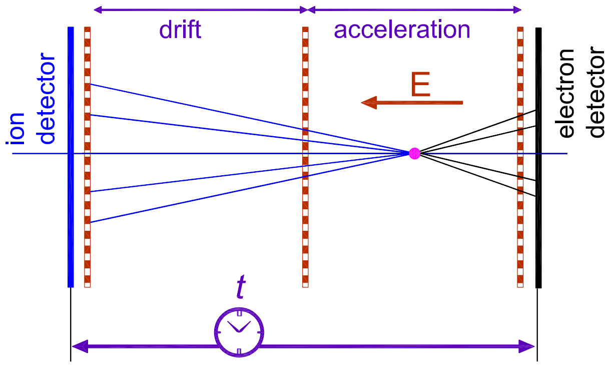

Figure 2.1: Principle of time of flight spectrometer based on electron ion coincidence. The acceleration stretch is labelled s, and the field free drift stretch is labelled D in the text.

and drift tube, D, which is maintained as field free region. The resolution of this TOF mass spectrometer is controlled mainly by the length of the flight tube. The ions formed in the interaction region, in the presence of an electric field (E_s), are accelerated towards the drift tube. Ions are time separated on the basis of mass by charged ratio, as for a same charge the lighter mass ion reached first to the detector compares to the heavy mass ion. The flight time measurement can be triggered by the detection of the ejected electron, and stopped by the arrival of the ion at the detector placed at the end of the drift region. To derive the flight time of ions, consider an ion created in interaction region having charge q and mass m. Let us denote the initial velocity along the extraction axis by v_z. The time t_s taken by ion to reached the field free region can be obtain by given equation.

$$s = v_z t_s + \frac{1}{2}\frac{qE_s}{m}t_s^2 \tag{2.1}$$

Solving the equation 2.1 gives the time-of-flight of ion in extraction region

$$t = \frac{-p_z/m + \sqrt{[p_z/m]^2 + (qE_s/m)s}}{qE_s/m} \tag{2.2}$$

In the field free region (drift tube), the time taken by ion is

$$t_D = \frac{D}{\sqrt{[p_z/m]^2 + (qE_s/m)s}} \tag{2.3}$$

The total time taken by ion to reached the detector $t(= t_s + t_D)$ is given by

$$t = \frac{-p_z/m + \sqrt{[p_z/m]^2 + (qE_s/m)s}}{qE_s/m} + \frac{D}{\sqrt{[p_z/m]^2 + (qE_s/m)s}} \tag{2.4}$$

This equation is the general flight time equation in which most of the experimental quantity such as D, E_s and s are known. For zero energy fragments, $p_z = 0$ and this equation will be converted in form as

$$t = A + B\sqrt{m/q} \tag{2.5}$$

where A and B is depend on on the known experimental quantity. The equation 2.5 is known as calibration equation. The use of this equation is discussed in data analysis chapter. Here, we would like to introduce concepts such as the space focusing condition which is useful for designing the TOF spectrometer, and resolution of spectrometer which depends on various factor. Details about the space focusing condition and the resolution are discussed next.

Space focusing condition

The over-all resolution of time-of-flight spectrometer is affected by the initial spatial spread (size of interaction region) and energy distribution of the created ions. The effect due to the space distribution can be minimized by a method known as a space focusing, in which the ions formed at different points of the source region have approximately the same flight times. Let s_0 be the center of the source region and Δs the diameter of the source volume. The maximum flight path difference occurs between two ions with zero initial energy formed at $s_{max} = s_0 + 0.5\Delta s$ and $s_{min} = s_0 - 0.5\Delta s$. These two ion gain different velocities due to the potential difference. The focusing condition implies that by combination of the parameter determining the flight time (s, D and E_s) which minimize the flight time difference between two ions formed at s_{max} and s_{min}. Its means that the mathematical condition must be satisfy $\partial t/\partial s = 0$. The optimal length for the drift tube with given s, d and E_s can be found by setting $(dt/ds)_{0,s0} = 0$. The new equation will be

$$D = 2s_0\sqrt[3]{k_0}\left(1 - \frac{1}{\sqrt{k_0 + \sqrt{k_0}}}\right)\frac{d}{s_0} \tag{2.6}$$

This is a very important and useful condition for designing the single field linear time of flight spectrometer. Our TOF-MS is designed to satisfy this condition.

Mass resolution

Mass resolution of time-of-flight mass spectrometer (TOFMS) is define as follows: Two adjacent mass peaks with masses m and $m + 1$ are resolved, if their time separation T_{m+1} - T_m is greater than or equal to ΔT, which is the full width half maximum of mass profile. The mass resolution depends on many factors, like source size, initial kinetic energy distribution and electronics. The source size effect can be minimized by space focusing. The upper limit on mass resolution based on the single field TOF spectrometer design under space focusing condition, as defined by Wiley and McLaren [Wil55], as

$$M/\Delta M = 16[s/\Delta s]^2$$

In present setup, the value of source extent (Δs) is 2 mm and an extraction length s is 110 mm. The mass resolution limit due to spatial spread

$$M/\Delta M = 48400$$

The second factor affecting the resolution is the initial kinetic energy distribution, which leads to broadening of the mass peaks and under certain conditions, even split them into two separate components. This can be understood by considering two ions originated at the same initial position with their velocities opposite to each other. One is directed to detector side and other one moves first away from it, stops and returns due to the applied field. As a consequence, the two ions have different flight-times to the detector. The time difference between ions moving parallel to detector and anti-parallel to detector would be

$$\Delta T = \frac{2\sqrt{2mU_0}}{qE_s} \tag{2.7}$$

where q is the charge state, E_s the extraction field of TOFMS, m is the mass of the ion and U_0 is the initial kinetic energy.

The estimation of $M/\Delta M$ based on the initial kinetic energy width of the ions is not relevant to the present spectrometer, as the primary purpose of the present spectrometer is to measure the initial kinetic energy itself. However, there will be some broadening due to thermal energy spread of the parent molecules. At room temperature this spread is about 25 meV. For a N_2^+ ion, this leads to a time spread of about 8 ns under the usual operating conditions.

We have discussed the details about the time-of-flight mass spectroscopy (single field-TOF) which is the essential technique of complete recoil ion momentum spectrometer. Next, we discuss how, if the position of arrival of the ions is known, we can get the complete ion momentum. The details about position sensitive detection is left to a later section.

2.1.2 Ion momentum imaging

Apart from the motion of the ions in a TOF spectrometer along the axis, ions suffer a deviation transverse to the field direction due to the *transverse components* of their momentum. As a result the ions fall at different positions on the detector, as shown in Figure 2.2. If the position of arrival, or the spatial deviation is known besides the TOF, we can obtain the initial momentum component of that ion. The 2-Dimensional image of all charged particle is referred to the charged particle imaging. The various kinematic information is stored within this image and the flight time distribution. The method of deriving the expression for momentum components are given in the next section.

2.1.3 Construction of momentum vectors

The kinematic parameter such as momentum components can be obtained from recorded coordinate and flight time information of fragments. Expres-

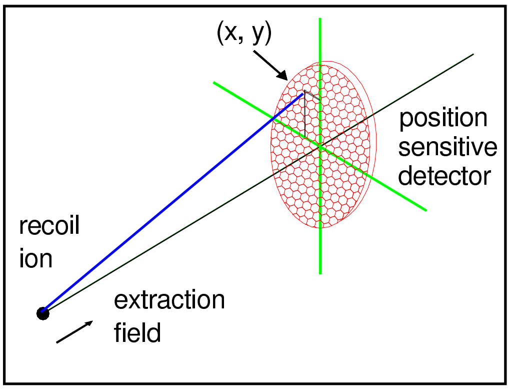

Figure 2.2: Principle of momentum imaging. The spatial momentum components, P_x and P_y are obtained from measured position coordinate of each fragments. The position resolution is 0.25 mm.

sion for z-components momentum can be obtain from equation 2.4. The time-of-flight, t_0 for ions which have zero initial energy is given by

$$\mathrm{t}_0 = \sqrt{2m}\left[\frac{\sqrt{qsE_s}}{qE_s} + \frac{s}{\sqrt{qsE_s}}\right] \tag{2.8}$$

In case of $\mathrm{p}_z^2/2\mathrm{m} \ll \mathrm{qE}_s$, the time difference between the zero energy and non-zero initial velocity ions can be written in a simplified form. From the equation 2.4 and equation 2.6, we get

$$p_z = qE_s(t_0 - t) \tag{2.9}$$

This is the expression for obtaining the $z-$component momentum vector. It is noted that this z-components is only the first order term which is dominant and good enough. The other terms are neglected. Once the flight time of the fragments are known in addition to the position information, the other momentum components can be obtained. The principle of obtaining the $x-$ and $y-$ component momentum from observed position information of fragment is shown in Figure 2.2. Using the flight time information and position information, for a given fragments having mass m, the momentum components parallel to detector plane and perpendicular to the time-of-flight axis are given by following expressions:

$$p_x = m \times (x_0 - x)/t \tag{2.10}$$

$$p_y = m \times (y_0 - y)/t \tag{2.11}$$

where (x_0, y_0) is the centroid of the interaction volume projected on the detector plane. The each components of fragments can be obtained by above expression and the further analysis are carried out from them. During momentum imaging analysis only those counts are taken which satisfied the time sum condition. x_0, y_0 are obtained from the observed image. Thus the momentum components are basically calculated by simple programming which extract the position coordinate information and time of each fragments. The t_0 information for each species is used to assign the mass of the ion, and to determine the p_z momentum components. The one-to-one assignment of t_0 and m/q is done based on the TOF spectrum alone, and then passed as parameter to the rest of the program for momentum calculations.

2.2 Multi-particle coincidence technique

In most of the molecular fragmentation, more than two fragments ejected may have different intrinsic parameter such as mass and velocity. The ions ejected from one dissociative event carry valuable information about the precursor state. Only detection of these ions does not give the information

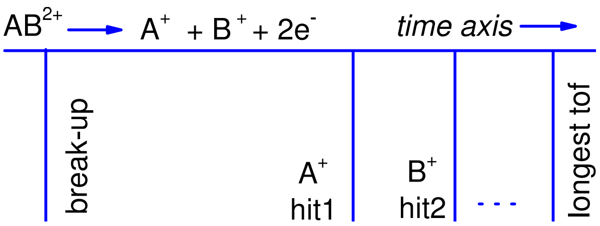

Figure 2.3: Principle of multi-particle coincidence technique. The longest time in present set-up is 32 μs. The time resolution is 1 ns

Table 2.1: Schematic representation of list mode events. The flight time and position of each charged fragments are recorded in the form of this table. During analysis the event list can be sorted out after acquisition is over and can use for calculating the other parameter such as momentum components, kinetic energy, angle between fragments and so on.

Event number	Ion1	Ion2	Ion3	Ion4
$\dots$	$\dots$	$\dots$	$\dots$	$\dots$
501	$(t,x,y)_{501,1}$	$\dots$	$\dots$	$\dots$
502	$(t,x,y)_{502,1}$	$(t,x,y)_{502,2}$	$(t,x,y)_{502,3}$	$\dots$
503	$(t,x,y)_{503,1}$	$(t,x,y)_{503,2}$	$\dots$	$\dots$
504	$(t,x,y)_{504,1}$	$\dots$	$\dots$	$\dots$
505	$(t,x,y)_{505,1}$	$(t,x,y)_{505,2}$	$\dots$	$\dots$
506	$(t,x,y)_{506,1}$	$(t,x,y)_{506,2}$	$(t,x,y)_{506,3}$	$(t,x,y)_{506,4}$
$\dots$	$\dots$	$\dots$	$\dots$	$\dots$

about particular event. There may be many distinct events which are ejecting same ion. Any mass peak in mass spectrum is the evidence of this. If the multiple ions are coming from same events then the flight time of any two fragments may have the correlation in the ion-ion flight time plot. This map is referred to as the correlation map. If there are many events and in measurement technique is not capable to detect ion in time sequence then the correlation will not be observed in this map. The technique which measures the ions signal in time sequence is refer to the coincidence technique, similarly, the detection of multi-particle in time sequence is known as multi-particle coincidence technique. In order to distinguish between events leading to one, two or more ions, a time ordered detection (and recording) of each fragments ejected from the event is necessary. This is done by using the ejected electron as a trigger or time start and ion detection used as multi-stop. The principle of multi-particle coincidence technique is shown in Figure 2.3. The ion detected first by ion detector is refer as hit1 and other ion detected after the detection of first ion is refer to the hit2 and so on. This technique is very useful for detecting the various dissociative channels. The our present detection technique also have the facility to record position and flight time information of each fragments for each event and listed it in proper manner which is known as list mode data. The form of list mode data file which stores the data during data acquisition is shown in Table 2.1. It is clear that the position as well as flight time information of each ions which are detected in coincidence are recorded as an event by event data and saved as a list.

2.3 Experimental setup

The results reported in this thesis were carried out using the Recoil Ion Mass Spectrometer (RIMS) setup. The spectrometer is housed in high vacuum chamber. Briefly the set-up consists of an electron beam, an effusive molecular beam which serves as the target in a crossed beam geometry and electric field assembly. Before discussing the details about the principle of time-of-flight mass spectrometer, multi-hit technique and construction of momentum vector, we give a brief introduction to the various part of the experimental set-up. Sketch of the spectrometer is shown in Figure 2.4.

2.3.1 Interaction region and collision geometry

The region in which the projectile beam and molecular jet interact is known as interaction region. In this set-up, the cross-beam geometry have been used. The interaction between electron and molecule take place in uniform electric field. The optimization for minimum overlap volume would be the challenging task because the electron beam trajectory is affected by electric field within the interaction region. To get rid of this problem we have used an additional electrode (called the compensating plate) to steer the electron

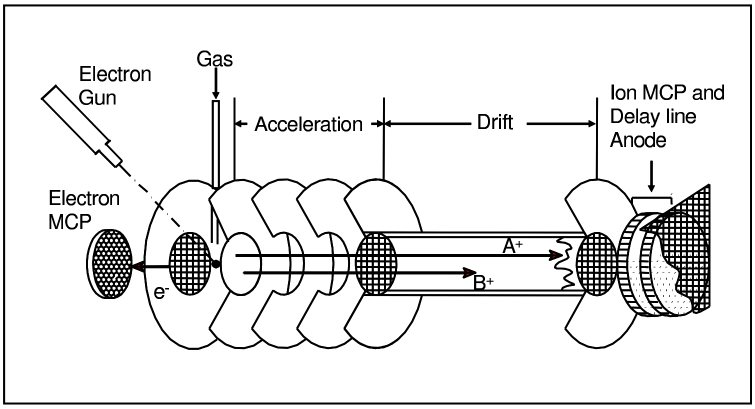

Figure 2.4: Sketch of the spectrometer. The cross-beam geometry for collision between the electron and targets molecules is shown clearly. The electron gun, the gas targets, acceleration region and drift tube, electron and ion detectors are shown. The accelerating field is generated by holding the rings in a potential divider arrangement, creating a uniform electric field in the gaps.

beam through the electric field with optimization of overlap with the target beam [Sha05]. The final optimization has been done by minimizing the FWHM of TOF profile of parent ion. The minimum value of FWHM of N_2^+ ion TOF profile is 8 ns which has achieved by fine control of horizontal, vertical deflection voltages of electron gun and the voltage of compensating plate. For good optimization, the FWHM should be small and position image must have highest intensity at center of image spectra.

2.3.2 Molecular beam

Effusive molecular beams are commonly used in collision experiments. The molecular beam is generated by passing a gas or a vapor through a non-magnetic stainless-steel capillary. The diameter of capillary is 0.15 mm and length is 12 mm. The capillary is joined to a 1/4″ diameter pipe with 136 mm length. The details about the gas line, capillary assembly with flange is shown in Figure 2.5. The two gas line shown in this Figure are for two differ-

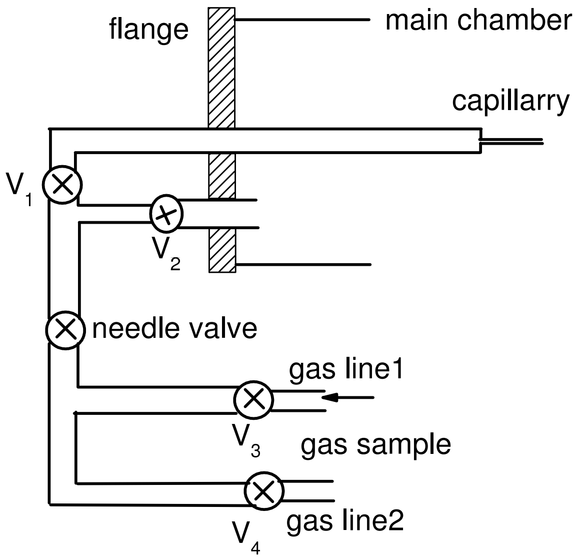

Figure 2.5: schematic view of gas line. The V_2,V_1,V_3 and V_4 are the safety valve. The needle valve is used to control the gas flow. The gas pressure at the time of experiment in gas line are kept of the order of 1-3 mbar and pressure in main chamber is of the order of 10^{-7} mbar.

ent purpose. One of the gas line is preferentially used for standard sample which is requires only for calibration and other gas line is for sample/gas of interest. The sample cylinder is connected with either of the gas line. Before the cylinder valve is opened, the evacuation of gas line is carried out to removed the residual gas. Before starting the experiment the evacuation with bake out of gas line is done. During evacuation of this line the vacuum achieved is 3.0×10^{-3} mbar. The gas line pressure during experiment is of the order of 1–3 mbar and the vacuum in main chamber is of the order of 2.0×10^{-7} mbar. Due to large pressure difference the gas jet is formed in the main chamber. Since distance between the line of electron beam and the tip of the needle is less than 3 mm, the divergence of molecular jet will be very small.

2.3.3 Electron gun

In our experiments, we have used electron gun to produce the electron beam. An electron gun is an electrical device that generates electrons and focuses them into a narrow beam with a well defined mean kinetic energy. Generally, the electron generation is either by a directly heated filament made of an oxide-coated metal with low work function, such as tungsten

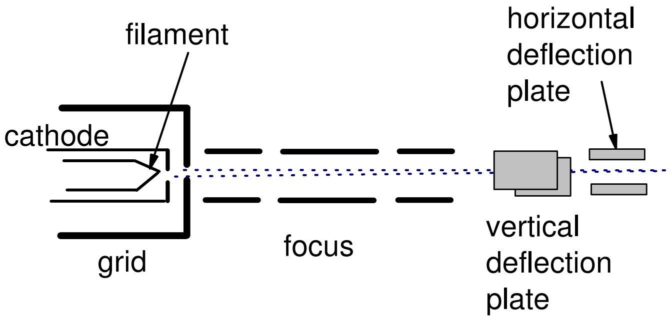

Figure 2.6: Schematic diagram of the electron gun we have used. In our experiment, the applied voltages are: at cathode = -1300 V, grid = -1250 V and focus is set at -850 V. The deflection plate voltages have been set to get a well defined cross-beam geometry. The horizontal and vertical deflection fields are of the order of 10 V/cm.

or rhenium or an indirectly heated cathode. Since the generation of electron is thermionic in both cases, the inherent spread in thermal energy of the electrons may affect the energy resolution. It is found that the magnitude of the thermal energy spread increases with the emitting surface temperature. The spread can be reduced by operating the filament at low temperature. At low temperature the intensity of emission current reduces and the pattern can be understood by Richardson equation [Ric12, Dus23]. To compensate the reduction in emission current density at lower temperature, a material of lower work function are normally used. The typical energy resolution for both the directly heated and indirectly heated electron source is of the order of 0.5 eV. However, the energy spread of the beam as it emerges from the gun is much larger.

We are using commercially available heated cathode thermionic emission electron gun. The details about the various parts of the electron gun is shown in Figure 2.6. The control grid is a hollow metal tube placed over the cathode. A small opening is located in the center of a baffle at the end opposite the cathode. The control grid is maintained at a negative potential with respect to the cathode to keep the electrons bunched together. The anode is at a positive potential with respect to the cathode and the large electric field pulls electrons through the aperture in the grid. Because the grid is near the cathode, it can control the number of electrons that are emitted. As in an ordinary electron tube, the negative voltage of the grid can be varied either to control electron flow or stop it completely. The intensity of the electron is controlled by the voltage on the control grid. The electrons are focused by Einzel lens. The electron beam can be swept in the transverse direction by electrostatic deflectors. At the focal spot the sweep is about 20 mm. The focal length can also be varied between 150–200 mm from the exit aperture. Coarse tuning of the beam is done by observing the beam spot on a fluorescent screen, and fine tuning is done by the TOF and position spectra.

2.3.4 Faraday cup

The Faraday cup is the metallic cup constructed to collect charged particle in vacuum. The measured current used to determine the number of ions or electrons hitting the cup. When a beam of charged hits the Faraday cup it gains a small net charge while the charged particles are neutralized. The cup can then be discharged to measure a small current equivalent to the number of impinging ions. The schematic of the Faraday cup we have used in our experiment is shown in Figure 2.7. The length of this cup is 50 mm and diameter is 20 mm. The tube is mounted on one of the flange

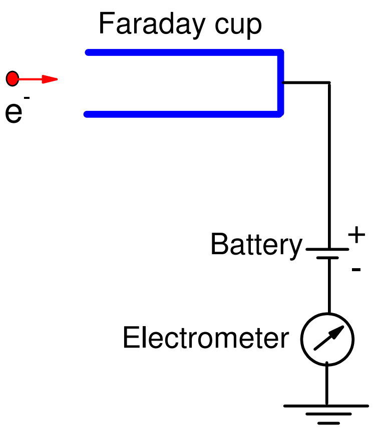

Figure 2.7: schematic of the Faraday cup we have used. The 28.0 Volt battery have been used. The details about the size is discussed in text. During optimization of experimental set-up, we maximize the FC current. Most of the experiment have been performed at 5 pico Amp of electrons beam detected by Faraday Cup.

of the main chamber by Teflon supports. Thus the Faraday cup is isolated from the main chamber. The electron beam coming from the electron gun passed through the interaction region and falls on the inner copper tube (Faraday cup) which gets collected. This current is measured by the electrometer. Positive voltage is applied on the collector to prevent the escaping secondary electrons from the tube. Without this bias, the secondary electrons could travel back and forth giving rise to false signal for time start in ion detection. Also, this false signal directly contributes in the background counts. During experiment, this cup is used to monitor the electron beam.

2.3.5 Detectors

In this experimental set-up, separate micro-channel plate (MCP) detectors have been used for detecting the electrons and ions which are ejected from the interaction region. A micro-channel plate is a slab made from highly resistive material of typically 2 mm thickness with a regular array of tiny tubes or slots (micro-channels) leading from one face to the opposite, densely distributed over the whole surface. The microchannels are typically about 10 micrometer in diameter and spaced apart by about 15 micrometers, they are parallel to each other and make a small angle to the surface ($\sim 8^\circ$ from normal). The micro-channel plate is shown in Figure 2.8.

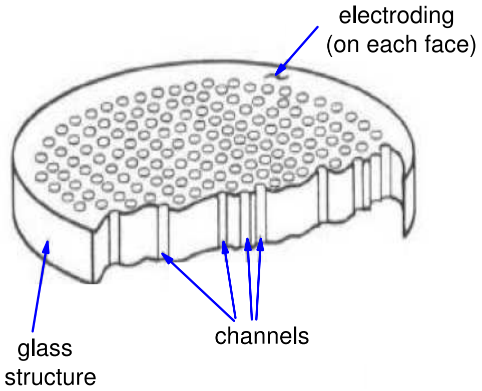

Figure 2.8: A microchannel plate. Details about the size, channels, diameter of channels and angle of these channels with respect to the surface are discussed in text.

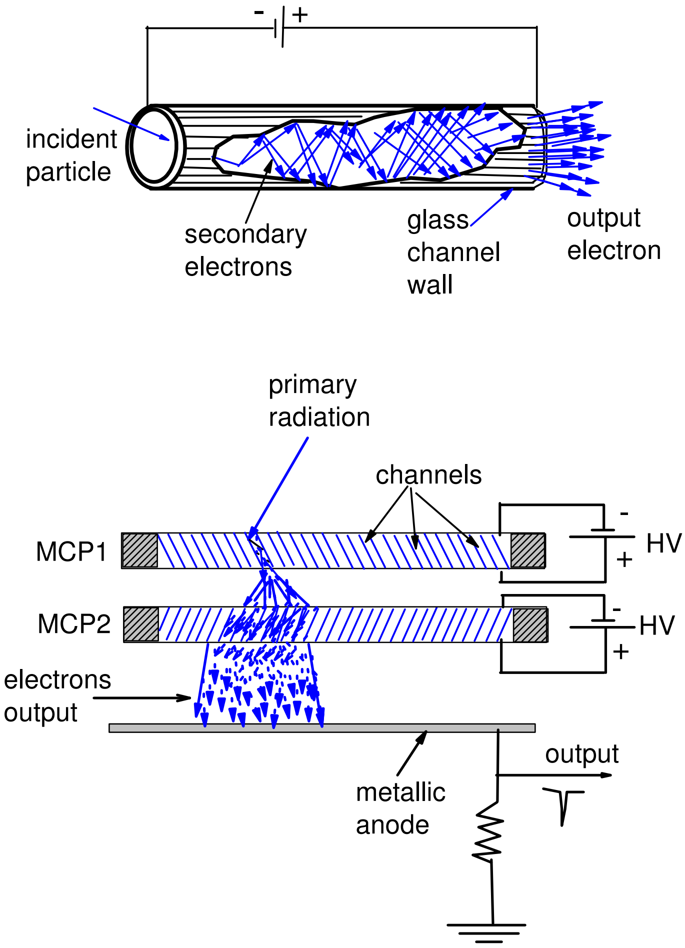

Figure 2.9: [top] Straight single electron multiplier or single channel.[bottom] Chevron operation of two MCP. The output signal is taken from the anode which is grounded with high resistance. The electron flux increased in this operation.

For understanding the working principle, the single channel and the complete circuit is shown in top panel of Figure 2.9. The incident particle or photon enters one of the channels through a small orifice is guaranteed to hit the wall of the channel due to the channel being at an angle to the plate. The impact starts a cascade of electrons that propagate through the channel, which amplifies the original signal by several orders of magnitude depending on the electric field strength and the geometry of the micro-channel plate. It is noted that after the cascade, the microchannel takes time to recover (or recharge) before it can detect another signal. The flux of electrons exit the channels on the opposite side where they are themselves detected by additional means, often simply a single metal anode measuring total current. In this set-up, the MCP detectors consist of two microchannel plates with angled channels rotated 90^0 from each other producing a chevron (v-like) shape. The Chevron operation of two MCP and circuit is shown in bottom panel of Figure 2.9. In this configuration, the plates are individually operated at gains the 10^4 range. It is clearly shown that the primary incident radiation or charged particle create secondary electron in one channel (single electron multiplier tube) that exit the first plate start the cascade in the next plate. The advantage of the chevron MCP over the straight channel MCP is significantly more gain at a given voltage.

2.3.6 Position Sensitive Detector

From the position information of charged fragments one can knows the spatial spread in the trajectory of ions which can converted into the momentum components of fragments. For this purpose, the electron shower from the back of the MCP pair is made to fall on a position sensitive anode. Various types of position sensitive anodes are commercially available. The wedge and strip anode and delay line anode can be directly coupled to a MCP. The principle of these position sensitive anodes are discussed below. We have used the delay line anode in present set-up. Another type of position sensitive anode is a phosphor screen combined with a charged coupled device (CCD) camera. This scheme is not very useful in molecular imaging due to slow electronic readout.

Wedge and Strip Anode

The Wedge and Strip anode offers good spatial resolution and fast timing signal. For details about this detector see [Lap86, Zhe08]. In brief, the wedge and strip structure is shown in Figure 2.10. The segmented anode is consist of electrically separated area with a wedge and strip structure at typical periodicity of 1.5 mm. Since the area of the wedges and stripes depends linearly on the x and y position, the pulse hight of the signals picked up at both electrodes are proportional to the position of the charged cloud centroid. To extract the position information the pulse height of the wedge and stripe segments have to be normalized to the collected total charge which varies from event to event. It is given by the pulse height sum of all electrodes, the wedge, the strip, and a meander structure that fills the area between the first two. All these signals are amplified in separate charged sensitive preamplifiers and recorded by analog to digital converter. The position information is obtained from the measured pulse heights reflecting the amount of charge collected by the wedges Q_w, the stripes Q_s and the meander, respectively

$$x \propto \frac{Q_S}{Q_S + Q_W + Q_M} \tag{2.12}$$

$$y \propto \frac{Q_W}{Q_S + Q_W + Q_M} \tag{2.13}$$

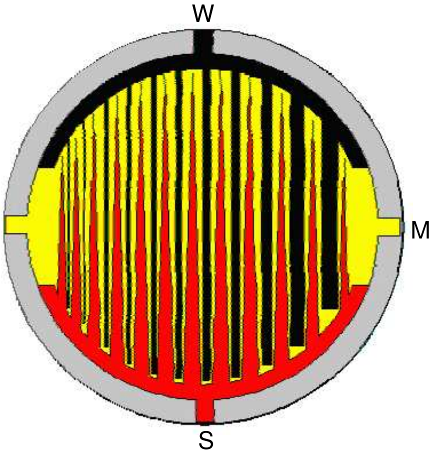

Figure 2.10: Wedge and strip anode. The widths of the wedges and strips vary linearly with the x and y coordinates, respectively.

Delay line anode

The delay line anode is a unique technique which can be use to extract the position of charged cloud centroid with good position resolution. The side and top view of the delay line anode and MCP configuration in usual delay line detector is shown in top panel of Figure 2.11, and the principle of this position sensitive detector is shown in bottom panel of the same figure. For details about the delay line anode detector can be found in literature [Spi01, Jag02, Cza07]. The delay line anode consists of two set of long wire that is wound in many loops around a rectangular support with a wire spacing of the order of 0.5 mm. One set of wires is wound perpendicular to other set of wire. Each set of wire give the information about coordinate. In this technique, the position information is encoded by the measurement of time a signal needs to travel along these wire. The time difference between the signals arriving at both ends of the wire is proportional to the position coordinate of the charged cloud centroid. The time signal at both ends extracted by both set of wire gives the coordinate information. Although one wire per coordinate is in principle sufficient to get the position, there are serious pickup problems associated with a single long wire. Instead a pair of wires is used for each coordinate. Both cables pick up an identical noise via capacitive coupling with the surrounding. Their signal differs only when a real charge is deposited on one but not on the other wire. To ensure that the only one wire collects the electrons from the cloud it is biased with a more positive potential and second wire is basically used for monitoring the noise. The end of the these cables are fed into a fast differential amplifier which subtract the noise from the signal. The differential signal allows us to determine the time difference between both ends of the cable. These signal is used for further signal processing and read out. From the collected timing information the x and y coordinate can be obtained by

$$x = (t_{x1} - t_{x2})v_{\text{signal}}, \quad y = (t_{y1} - t_{y2})v_{\text{signal}} \tag{2.14}$$

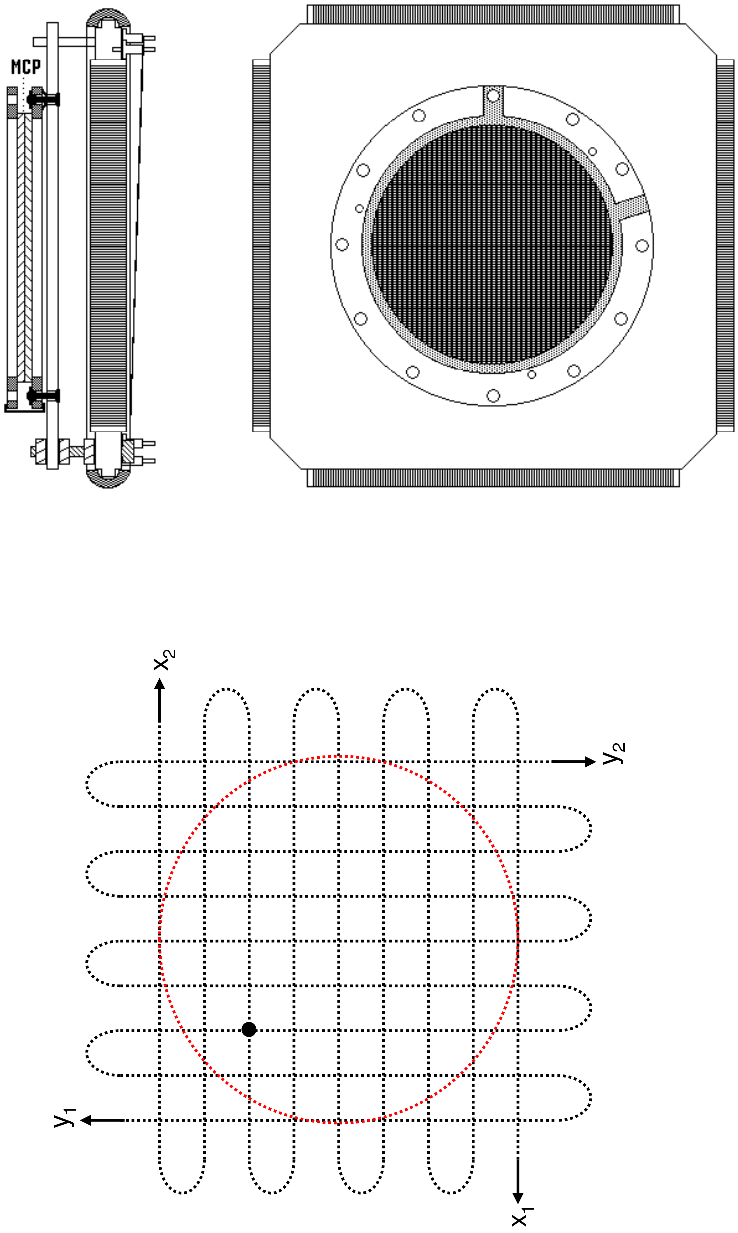

Figure 2.11: [Top] Complete configurational side and top view of delay line anode detector. [Bottom] Operation of delay line anode as a position sensitive detector

It is noted that the sum of the travel times to the two ends of the cable for x and y coordinate are constant for a given length of wire. This is a very useful parameter for obtaining the true counts or signal. This is known as time-sum condition.

2.4 Data acquisition

The data acquisition in present set-up is based on six timing signal. One from the electron MCP and one from the ion MCP and four from the delay-line. The electron signal trigger to the five channels of TDC (LeCroy 133MTD). The first four channels are stopped by the delay-line signals and proving the position information about that ion. The fifth channel is stopped by the ion MCP signal which gives the time-of-flight. The longest waiting time for ion arrival is 32 μsec and the time resolution of TDC used in this set-up is 500 ps. When all channels are active then we can perform acquisition with maximum event rate of 1.2 kHz. In practice, the false coincidence counts will be recorded if the event rate is high. Usually we keep the event rate as low as possible. The most of the data presented in this thesis is acquired with event rate ranging from 100–300 Hz. In this case the false coincidence counts are expected to be low and with time sum condition we can get only true coincidence counts from list mode file.

The outputs of the five channels for each events are converted to a digital signal and stored as a list on a computer disk. The TDC has a PC interface written in the MS-Visual C++ language. The program is known as Cobold-PC, which stands for "Computer Based Online-offline Listmode Data Analyser". List mode is a special technique used in collision physics. In this mode, all acquired information (named coordinates in Cobold-PC) is stored event by event in a data list. The original Cobold-PC program is meant for imaging, using the four delay-line signals. The program was modified to accept five inputs so that the vital TOF information could also be recorded simultaneously with the position [Sha07].The event list adapted to our requirements contain (x_1,x_2, y_1, y_2) and t , entries, obtained from the delay-line anode and the electron-ion coincidence respectively.

2.5 Summary

We have discussed various aspects of experimental set-up. The principle, technical detail of each components of the recoil ion momentum spectrometer have been given for understanding the measurement method. The method of obtaining the momentum components of the ions are described in detail. The multi-ion coincidence technique which is vital for knowing the dissociative ionization channels of a molecule is also discussed. Finally, the data acquisition and data storing method have been described. The figure of merit of our recoil ion momentum spectrometer is discussed in the Appendix A.

Chapter 3

Data Analysis Methodology

In this chapter, the data analysis methodology is explained. Many useful informations such as the flight time distributions of different species, time correlations in product arrival times of various ions in a single fragmentation event, identification of dissociative channels, kinetic energy release and angular distribution of the products are arrived at by systematic reduction of the list mode data. For demonstrating the methodology of data analysis, we have chosen the case of dissociative ionization of the simple triatomic molecule SO_2. *The data analysis scheme used for other targets is essentially the same as discussed in this section.*

3.1 Calibration of the spectrum

To get a precise calibration of the TOF spectrum, it is necessary to have a many known mass peaks as possible over the entire range of masses. This is easily obtained by recording a spectrum of Xe ions, which is expected to show multi-ionised states and six isotopes. Various experimental parameters such as the applied voltages to extraction plate, compensating plate, vertical and horizontal deflection plate of electron gun and voltage at focus terminal of electron gun etc., are optimized for the best performance (best mass resolution and signal to noise ratio) of the complete setup. These influence the overall TOF spectrum, so it is necessary to record a standard spectrum once the parameters are optimized. After the optimization of the set-up, these parameters are kept fixed for all the rest of experiments. The time-of-flight [TOF] spectrum of Xe is shown in top panel of Figure 3.1. Mass peaks lead to multiply ionized Xe atoms and its isotopes are also seen in TOF spectrum. Note that all isotope peaks of Xe are well resolved.

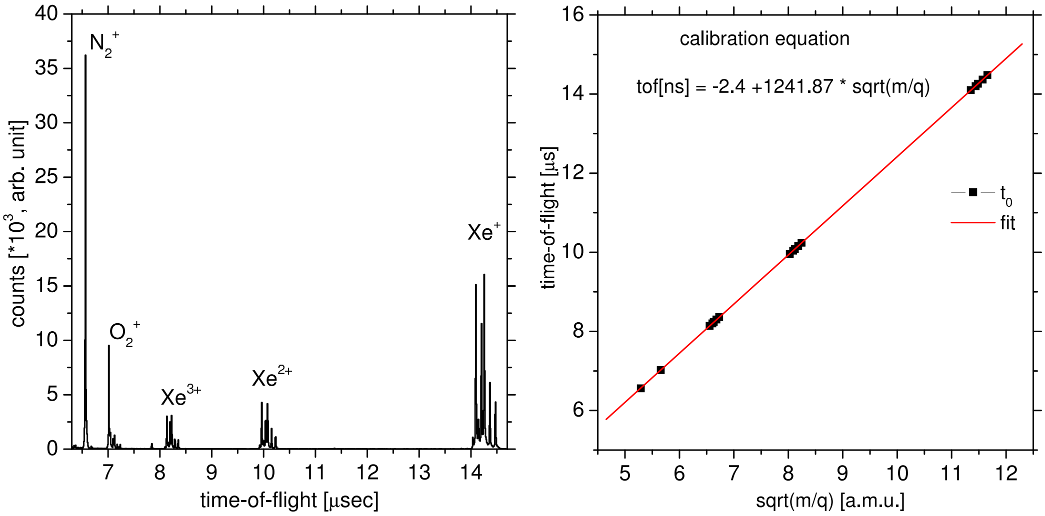

Figure 3.1: [left] Time-of-flight spectrum of Xe. It is noted that the Xe have many stable isotopes. The six peaks in each profile of Xe^{n+} (n=1,2,..) are due to the isotopes of Xe. [right] Plot for calibration equation, obtained by linear fit of time-of-flight vs. $\sqrt{m/q}$

Oxygen and nitrogen were present in the gas as impurities and the mass peaks corresponding to parent molecular ions also are seen in the TOF spectrum. The broadening in TOF profile of any ion depends on the intrinsic momentum spread of fragments and instrumentation effect. For a given intrinsic momentum, the ejected ions in forward direction (toward detector) will reach the detector before the backward ejected ions. The charged fragments with zero momentum will be appear at the centroid of TOF profile. We denote t_0 the center of TOF profile. From the time-of-flight spectrum of Xe, the t_0 of all Xe^+, Xe^{2+}, Xe^{3+}, Xe^{4+} peaks and their isotopes are obtained. Since m/q of these ions are known, we can plot the TOF (t_0 of all peaks) vs $\sqrt{m/q}$ as shown in right panel of Figure 3.1. The linear fit through these point is used to get the calibration equation of the apparatus. If any experimental parameter changes during experiment then the re-calibration of the set-up for the new parameter is needed for which the Xe spectrum is acquired once again.

3.2 Ion-ion coincidence map

The ions of many body fragmentation will have correlated times of flight as they originate from the same dissociation event. The detection of several particles in a time ordered sequence triggered by single signal is called multi coincidence detection. In two-body break-up, the ion detected first is called hit1 ion and ion detected after the detection of first is called hit2 ion. The plot of time-of-flight of hit1 ion vs. time-of-flight of hit2 ion is called the pair coincidence or correlation map. For more than two-body break-up, the ion detection as third hit or fourth hit may be possible. In that case we can obtain the correlation map between time-of-flight of hit2 and time-of-flight of hit3, and so on. In fragmentation of polyatomic molecule, usually many distinct dissociative event occur. These events appear as islands in coincidence map due to bunching of the flight times of correlated ions. This island reflects the dissociative pattern. The identification of these islands

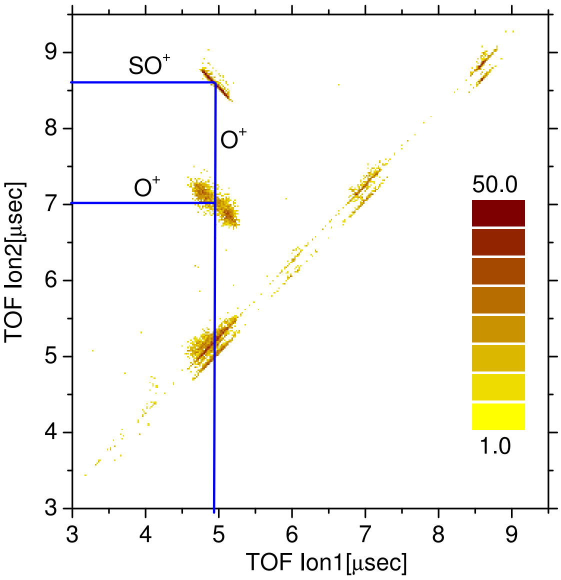

Figure 3.2: Ion-ion coincidence map of SO_2. The high energy electron (1300 eV) have been used to ionized the SO_2. Fragments are detected in time sequence. The islands O^+: O^+ and O^+: SO^+ are represents the two dissociative channels of SO_2^{2+}.

is accomplished on the basis of the m/q calibration equation. The intensity of the island represents the dominance of that particular dissociative channel. The details about the method for coincidence map analysis has been reported earlier [Mor00]. The coincidence map for dissociative ionization of SO_2 is shown in Figure 3.2. Two islands are appears in the coincidence map. The observed islands are O^+: SO^+ and O^+: O^+. These islands originate from doubly ionized SO_2 molecule. The information about two-body or many body break-up reaction can also be known from observed islands. For example, the island O^+: SO^+ is due to the complete two-body break-up of SO_2^{2+}. The reaction of this break-up is

$$SO_2^{2+} \longrightarrow O^+ + SO^+ \tag{3.1}$$

In a purely two-body break-up, only a single bond breaks, as seen in reaction 3.1. On the other hand the observed island O^+: O^+ is due to three-body break-up in which the third fragment may be either S^+ or S neutral. We have not found S^+ in time-of-flight of hit3 spectrum which indicate that the third fragment is neutral S atom. The corresponding break-up reaction for this island have two possibility, one is the sequential break-up of SO_2^{2+} as

$$\begin{aligned} \mathrm{SO_2^{2+}} &\longrightarrow \mathrm{O^+ + SO^{+*}} && (3.2) \\ \mathrm{SO^{+*}} &\longrightarrow \mathrm{S + O^+} && (3.3) \end{aligned}$$

The other possibility is the simultaneous break-up of both S–O bonds. The reaction for simultaneous break-up is

$$\mathrm{SO_2^{2+}} \longrightarrow \mathrm{O^+ + S + O^+} \qquad (3.4)$$

Which of these reactions has occurred can often be determined from an analysis of the islands in pair coincidence. The slopes and shapes of the islands bear definite signatures of the fragmentation dynamics. Following the prescription of Eland [Ela91], we can exploit the slope and the shapes of the coincidence islands to resolve the mechanisms of fragmentation of a molecular ion. For a one step, two-body decay ($2b$ decay), or a sequential decay in which a neutral fragment is detached in the first step and the charges separate in the second step (s_2 decay), the momenta of the ionic fragments are anti-correlated. The island shape is a rectangle with slope -1. For a sequential decay in which the charges separate in the first step (s_1 decay), the slope is $-(q_1/q_2)[(m_1+m_n)/m_1]$ or $-(q_1/q_2)[m_2/(m_2+m_n)]$, where the ions are labeled 1,2 in the order of detection, and n refers to the neutral fragment. The first value holds if the intermediate species is $(m_1m_n)^+$, while the second values holds if the intermediate species is $(m_2m_n)^+$. The shape of the island is a parallelogram, with one pair of opposite sides parallel to the t_1 or t_2 axes. The fourth type of decay is a fast, simultaneous, or a concerted (c) type, in which any arbitrary combination of correlated momenta may be found, and the islands may not have definite shapes. The shape and slope analysis of the island have been used in this thesis for knowing the types of fragmentation process.

3.3 Momentum maps and fragmentation kinematics

The information about the geometry of fragmenting molecular ion can extracted from study the three- or many body break-up of precursor by momentum measurement. The angular information of each fragments can be used to map the ejection pattern of the fragments. The visualization of two- and three-body break-up of precursor by momentum vectors are described in the next section.

3.3.1 Momentum analysis of two- and three-body break-up

From the observed complete momentum of each fragments we can visualize the ejection pattern of fragments in two-body or three-body break-up. For more than three-body break-up, visualization in a 2-D plot is difficult and other methods have been used [Tri96, Dor00, Sch07, Ren08]. In a momentum map, the ejection direction of any fragment taken as reference vector and the longitudinal and transverse momentum components of other fragments with respect to reference are plotted in 2-D plane. As an example, we condiser two-body break-up of SO_2^{2+} into O^+ and SO^+. In this case the ejection of SO^+ ion is taken as reference and the projection of momentum vector of O^+ ion is plotted in 2-D map, shown in Figure 3.3. In this map, the magnitude of SO^+ momentum is also shown. It is clear from this result that the O^+ ejection angle with respect to reference is 170°. Note that the ex-

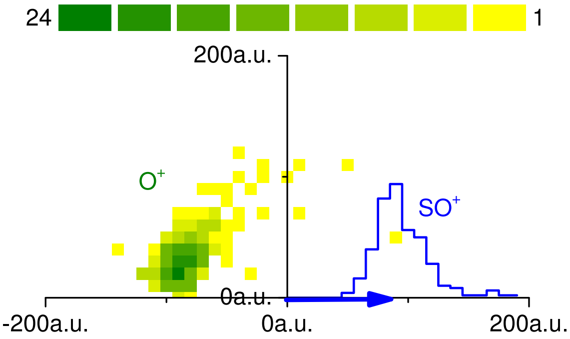

Figure 3.3: Momentum map of two-body break-up of SO_2^{2+}. Arrow is the indication of ejection direction of SO^+. The details about this map is discussed in text.

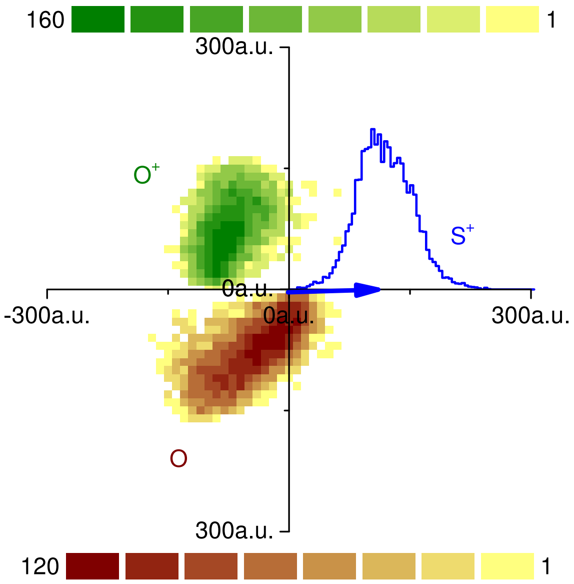

Figure 3.4: The momentum map of three-body break-up of SO_2^{2+}. The momentum components of O^+ and neutral O is plotted with respect to the reference(x-axis, ejection) S^+ ion. The momentum distribution of S^+ ion is also shown.

perimental limitation is 8°, thus, this map give clear picture of back-to-back ejection.

In the case of three-body break-up, the fragments may fly in any direction with respect to each other but they must to confined in one plane. Usually in molecular fragmentation, some of the fragments are neutral. Neutrals are not detected in mass spectrometer, thus the dissociative channels in which more than one neutrals are ejected can not be explainable. But in case of three-body break-up and when one of the fragments is neutral then the kinematic information about this ion can be obtained by applying momentum conservation. It is noted that some of the three-body reaction are sequential break-up. In that case that the process of second stage break-up is equivalent to two body break-up. The sequential as well as the concerted break-up can be also be identified from the momentum map. In the three-body momentum map, if we observe the back to back ejection of any two fragments and the third fragment is ejected at 90°, it indicates a two-step process. Momentum map for three-body fragmentation of SO_2^{2+} is shown in Figure 3.4. It is clear that the process is not sequential. Thus from the momentum map, we can know the type of process and the also the geometry of the precursor ion. The angular information between each fragments can transform into a polar plot which can be more useful for visualization of dissociative geometry of fragments. The details about the polar plot is discussed in the next section.

Geometry of precursor ion: Polar plot

In a polar plot, direction of ejection of one of the fragments is taken as a reference and the angular information of other two fragments are plotted with respect to reference. The peak in the angular distribution is the most probable direction of ejection of that ion. The broadening of this distribution may be large and depend on the slope of the repulsive state of precursor ion and also the various experimental parameter such error in momentum measurement can propagate in calculating the angle between two fragments. We have taken the three body break up of SO_2^{2+} into S^+, O^+ and O (neutrals) as an example. This break-up is the concerted process confirmed by the measurement of slope and shape of island in coincidence map. The momentum of each charged fragments are measured. The momentum of neutral O is calculated by law of momentum conservation. The momentum of neutral O is obtained by

$$\overrightarrow{P}_O = -(\overrightarrow{P}_{O^+} + \overrightarrow{P}_{S^+}) \tag{3.5}$$

where $\overrightarrow{P}_{O^+}$, $\overrightarrow{P}_{S^+}$ and $\overrightarrow{P}_O$, are the momentum of O^+, S^+ and O respectively. The angular distribution between each fragments are obtained from momentum information of each fragments. The polar plot for this dissociative channels is shown in Figure 3.5. It is clear that the O-S-O angle is $95^\circ \pm 8^\circ$. As we know from the literature that the O-S-O angle in ground state geometry of SO_2 is 119°. Thus, this method can be used to extract the information about the geometrical distortion. This method will be used for estimating the geometry of polyatomic molecular ion. The details about the geometry of molecular ion is discussed in Chapter 6.

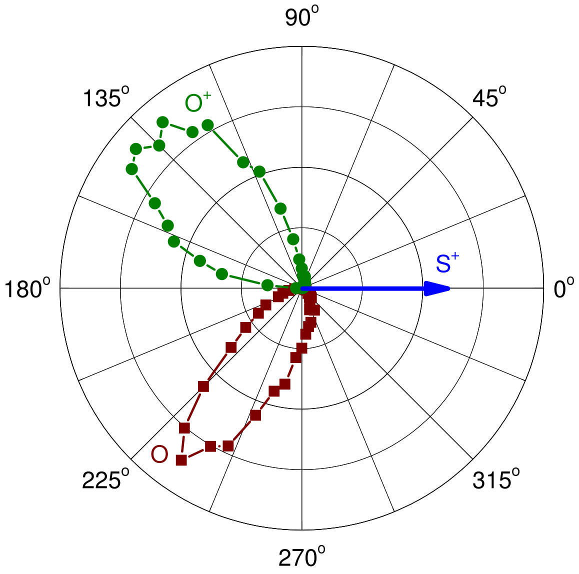

Figure 3.5: Polar plot of three-body break-up of SO^{2+}. In this plot, the ejection direction of S^+ is taken as reference and the angular distribution of other fragments are plotted with respect to that.

3.3.2 Kinetic Energy Release

The kinetic energy release is a measure of the the repulsive state potential energy surface [Tar00, Sie00, Raj06]. In dissociation of molecular ion, the excess energy is converted into the kinetic energy of fragments and the internal excitation of fragments. It is noted that the most of the energy is converted into the kinetic energy of the fragments. The schematic representation of molecular excitation, dissociation into two fragments and kinetic energy release is shown in Figure 3.6. The ground state potential energy curve and excitation to repulsive potential energy curve of doubly ionized precursor which dissociates into two charged fragments is shown in this Figure. One repulsive potential energy curve is also shown in the figure. In principle, many repulsive states are possible in a single precursor. The state accessed depends on the perturbation. The information about the various repulsive states of fragmenting ions are not known. Some of the excited state may also initiate the association reaction. Thus, the investigation of KER is very useful for understanding the fragmentation dynamics of molecules.

The KE distribution can be broadened, depending on the slope of repulsive state of precursor ion. In two-body Coulomb break-up, the poten-

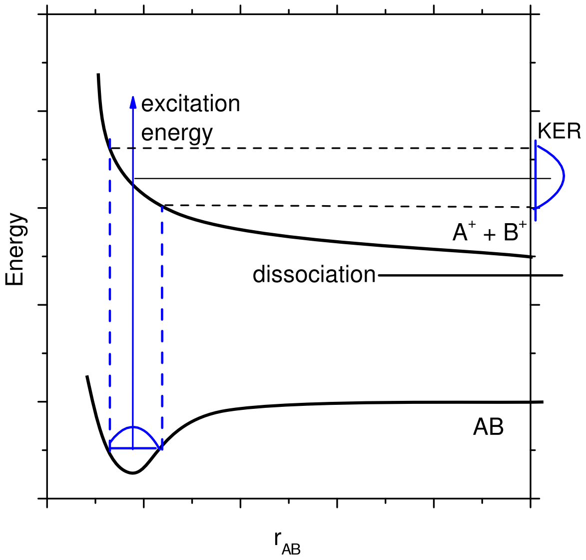

Figure 3.6: Schematic representation of kinetic energy release (KER). The excited energy state is the repulsive potential energy curve of dissociating precursor. The KER is the energy release by the precursor in form of kinetic energy of the fragments.

tial energy of repulsive state is form of q_1q_2/R, where the q_1, q_2 are the charges on fragments and R is the inter-atomic distance. This model can be used to explain the KER of complete Coulomb break-up. The details about the Coulomb break-up of molecular ions are available in literature [Vag89, Pos95, Cor96, Zha05]. The experimental limitations can also contribute to the broadening of the profile of the kinetic energy release. Experimentally, the kinetic energy of fragments can be obtained by measuring momentum of each fragment. For many body break-up, if p_i is the i^{th} fragment momentum and m_i is the mass of the same fragments, then the kinetic energy of this fragment $E_i = p_i^2/2m_i$. The kinetic energy release (KER) will be the sum of all kinetic energy. Here, an example of SO_2^{2+} which dissociates into S^+, O^+ and neutral O have been presented for exploring the methodology of KER investigation in molecular fragmentation. The kinetic energy release of SO_2^{2+} which dissociates into S^+, O^+ and neutral O, is shown in Figure 3.7. Note that neutral KE can also be determined by the momentum mapping technique. The observed KER is broad and the tail of this KER goes to 45 eV which possibly due to the nature of repulsive state. Further, in three-body break-up, the momentum sharing between the fragments increase the broadening and thus form a tail. The peak of the KER is at 11.0

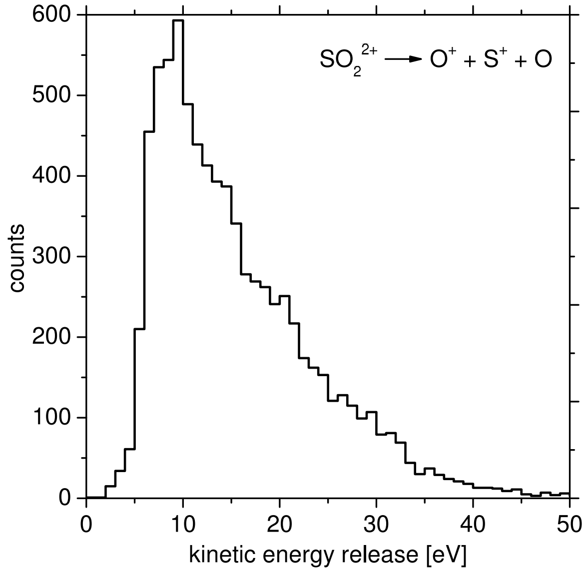

Figure 3.7: Kinetic energy release in dissociation of SO_2^{2+}. The KER is sum of the KE of S^+, O^+ and O. The KE of O is determined indirectly via the momentum conservation.

eV, which is the most probable height above the dissociation limit on the repulsive potential energy surface.

3.4 Summary

Various aspects of data analysis are described by taking the example of one atomic gas Xe (used for calibration) and one linear molecule SO_2. The method of calibration and identification of ions in time-of-flight spectrum are discussed. The method of analyzing the island appearing in the coincidence map and identification of dissociative channels of polyatomic molecular ion are described. Differentiation between various types of dication fragmentation sequences on the basis of the slope and shape analysis of island is explained. Analysis of the momentum map is presented, in particular the method of determining the kinetic energy of the undetected neutral is explained, and its use in deriving the kinetic energy release in a three-body break-up is emphasized. Further, for three-body reaction, angular distributions of the fragments are dwelt upon and their usefulness in visualizing the geometry of the fragmenting precursor is brought out.

Chapter 4

Association and Migration of Atoms during Fragmentation

Fragmentation is a process in which unstable molecular ions split into smaller molecular ions, or neutrals. It may so happen, that during fragmentation, two or more atoms within the same molecule may combine, leading to the formation of new species. Intra-molecular association is a rare event compared to the bond break-up reaction in fragmenting molecular ions. The molecular ions may have large number of repulsive excited states which eject the various types of ionic or neutral species. Excitation to some repulsive states may lead to ejection of associative fragments. Association is more common in polyatomic molecule, but in principle, can occur even in triatomic molecules depending on the perturbation and the nature of the excited states of precursor molecular ion. Although many attempts have been made to understand the association processes, it is not fully understood. In this chapter, we have investigated various aspects of intra-molecular processes, mainly in methane and its derivatives, as these species are expected to exhibit various aspects related to associative reactions. We refer to fragments formed by association of one or more atoms during the fragmentation of the parent molecular ion as associative fragments.

4.1 Associative fragments from linear and bent triatomic molecules

Association, in its simplest form, can occur in a linear or bent triatomic molecule. To begin, we have chosen one bent molecule (H_2O) and two linear molecules (CO_2 & CS_2). The likely association products are H_2^+, O_2^+ and S_2^+, respectively. The mass-spectrum of H_2O, CS_2 and CO_2 under 1300 eV electron impact is shown in Fig. 4.1, where evidence for H_2^+ and S_2^+ is seen. Such associations have been reported under various conditions [Smy33, Nag91, Kin08]. These molecular ions can only be formed when the terminal atoms come close together via bond bending. Since H_2O has a bent geometry in the neutral state, the excited state geometry may be more deformed than the ground state which induces the bond association reaction and formation of H_2^+ ion. The probability of association in bent triatomic molecules is expected to be larger than in linear triatomic molecules.

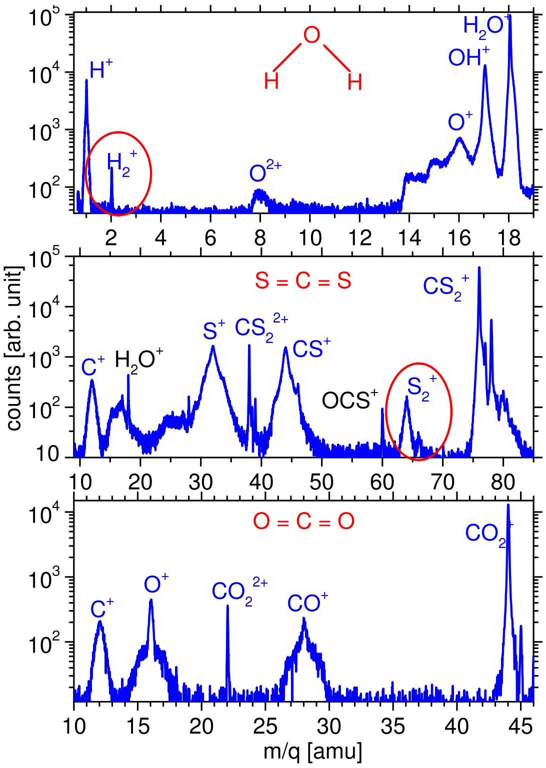

Figure 4.1: Mass spectrum of H_2O, CS_2 and CO_2 obtained by 1300 eV energy electron impact on these molecules. All experimental parameter during experiments are same for all molecules. The experiments were performed at low event rate (100-200 Hz). The H_2O^+ and OCS^+ (marked in black) in mass spectra of CS_2 are due to contamination in sample molecule.

The S_2^+ ion is detected in mass spectrum of CS_2 but the O_2^+ ion is not observed in mass-spectrum of CO_2. Since the ground state geometry of both molecule is linear, the possibility of fragmentation patterns are expected to be same. The observed associative product ion in CS_2 shows that the excited state geometry of singly or doubly ionized CS_2 is not linear but is deformed to a bent state which possibly initiates the association channel. We have found that the probability of observing S_2^+ from CS_2 and H_2^+ ion from H_2O, relative to the simple fragmentation (leading to H^+ or S^+), are roughly equal. We conclude that the geometrical deformation is responsible for association. The possibility of association reaction in polyatomic molecule such as CH_4 and atom substitution effect on associative reactions are discussed in next section.

4.2 Associative fragments from methane and derivatives

For the study of intra-molecular bond association in polyatomic molecule, the tetrahedral symmetric hydrocarbon CH_4 has been chosen in which all H atoms are geometrically equivalent. Formation of H_2^+ from CH_4 has been reported in the literature [Ben93, Wer03, Lun03]. Since distortion of the skeletal structure is likely to enhance the association reaction, we compare the associative ion yield from CH_4 with the yield from derivatives of CH_4 which already have a distortion from tetrahedral symmetry. This effect of *atom substitution in associative reactions* is investigated in CH_3Cl and CH_3OH. Note that both functional groups –Cl and –OH have large electro-negativity. This substitution changes the local environment of remaining H atoms, thereby affecting the association process. It is noted that the physical and chemical properties of CH_4, CH_3Cl and CH_3OH are different. We shall focus only the geometrical and atom substitution effect on association processes involving H atoms.

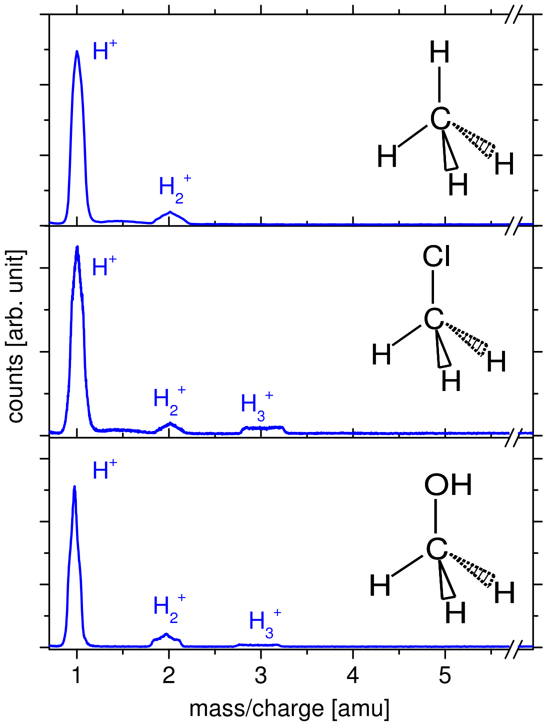

Figure 4.2: A partial mass spectrum of CH_4, CH_3OH and CH_3Cl under 1300 eV energy electron impact. All experimental parameter for these molecules are same during experiments. The experiments were performed under single collision condition and low event rates (100-200 Hz). The formation of H_3^+ ion is seen in mass-spectrum of CH_3OH and CH_3Cl.

Further, we have looked into the relative contributions, or *site-dependence* of the two functional groups CH_3– and –OH to the associative reactions in the CH_3OH molecule. This is a simple molecule which has two distinct chemical groups bearing H atoms.

4.2.1 Atom substitution effect in associative reactions

A partial mass-spectrum of dissociative ionization CH_4 molecule induced by electron impact is shown in top panel of Figure 4.2. The formation of H_2^+ is seen in this spectrum which is the evidence of atom-atom association. The partial mass spectrum of CH_3Cl and CH_3OH molecules is also shown in same Figure. It is clear from the observed mass spectrum of CH_3OH and CH_3Cl, that we have found the formation of H_2^+ as well as H_3^+ ions. It is noted that the associative ions can be formed from singly as well as doubly ionized precursor. We have no evidence of formation of triply ionized precursor in the triple ion coincidence map. The key feature in these spectra is that H_3^+ is formed from derivatives of methane, but not in methane itself.

precursors	H_2^+	H_3^+
CH_4^+	0.0033	–
CH_4^{2+}	0.0010	–
CH_3Cl^+	0.0014	0.0015
CH_3Cl^{2+}	0.0003	0.0005
CH_3OH^+	0.0099	0.0027
CH_3OH^{2+}	0.0013	0.0002

Table 4.1: Yield of H_2^+ and H_3^+ ions from singly and doubly ionized precursors normalized to the total ion yield from the particular molecule.

We can separate the ions from doubly and singly charged precursors by analyzing the list mode data and sorting out those events which have led to ion pairs. Events in which ion pairs are formed arise from doubly ionized precursors. Probability of associative ion ejection, relative to the total ion yield, from singly as well as doubly ionized precursor of CH_4, CH_3Cl and CH_3OH are listed in Table 4.1.

Note that H_2^+ can be formed in six equivalent ways (combinations) from CH_4 but in only three ways from CH_3Cl. In CH_3OH, there are six possible combinations but they are not equivalent. Similar considerations hold for H_3^+. With this in mind, we note from the table that the yield of H_2^+ (after taking into account the weight factors due to the various combinations of H atoms possible in the molecule) is roughly the same for CH_3Cl and CH_4. However, there is a large enhancement in case of CH_3OH. In case of triple association (H_3^+ formation), the enhancement due to the presence of –Cl and –OH radicals is pronounced. In fact, the presence of –Cl enhances triple association even more than pair association. This implies that deviation from tetrahedral symmetry in CH_3Cl^{2+} is very large and brings the three H atoms very close to each other. Similar distortion mechanism appears to be present in CH_3OH, but its effect is more favorable for pair association, than triple association.

4.2.2 Kinetic energy of associative fragments

The associative fragments may be ejected from various deformed geometrical states of the ionized methane and its derivative. As a result of substitution, the geometry as well as the energy level of the derivatives molecule are different than the methane. The fragmenting precursor may have many geometrically deformed molecular states which contribute to the formation of various associative fragments. The evidence of this may be found in the kinetic energy of the associative fragments. By measuring the kinetic energy of fragments, we can get an idea of the multitude of molecular states which contribute in formation of these ion. The kinetic energy distribution for H_2^+ and H_3^+ ejection is described in next section.

Kinetic energy distribution of H_2^+

The formation of H_2^+ ion from ionized methane may have different nature of ejection compared to its formation from methane's derivative molecules such as CH_3Cl, CH_3OH. Also, there might be different geometrically excited state which initiate the association in singly and doubly ionized precursor. The observed kinetic energy distribution of H_2^+ ion from singly and doubly ionized precursor of CH_4, CH_3Cl and CH_3OH is shown in Figure 4.3. The KED of H_2^+ ion ejected from singly ionized precursor is double peak structure. The double peak profile of KED of H_2^+ ion originated from singly ionized CH_4 precursor indicates the possibility of two molecular states of CH_4^+ ion.

If we compare the KED of H_2^+ ion ejected from the singly ionized precursor of CH_4's derivative such as CH_3Cl^+ and CH_3OH^+, the group specific association reaction can be distinguished. Since, H_2^+ ion can eject only from the methyl group of CH_3Cl^+ the single peak at low energy indicate the molecular state of CH_3Cl^+ during association in methyl group. The KED profile of H_2^+ ion ejected from CH_3OH^+ is the double peak structure. The first peak is due to the methyl group and higher energy peak is due to

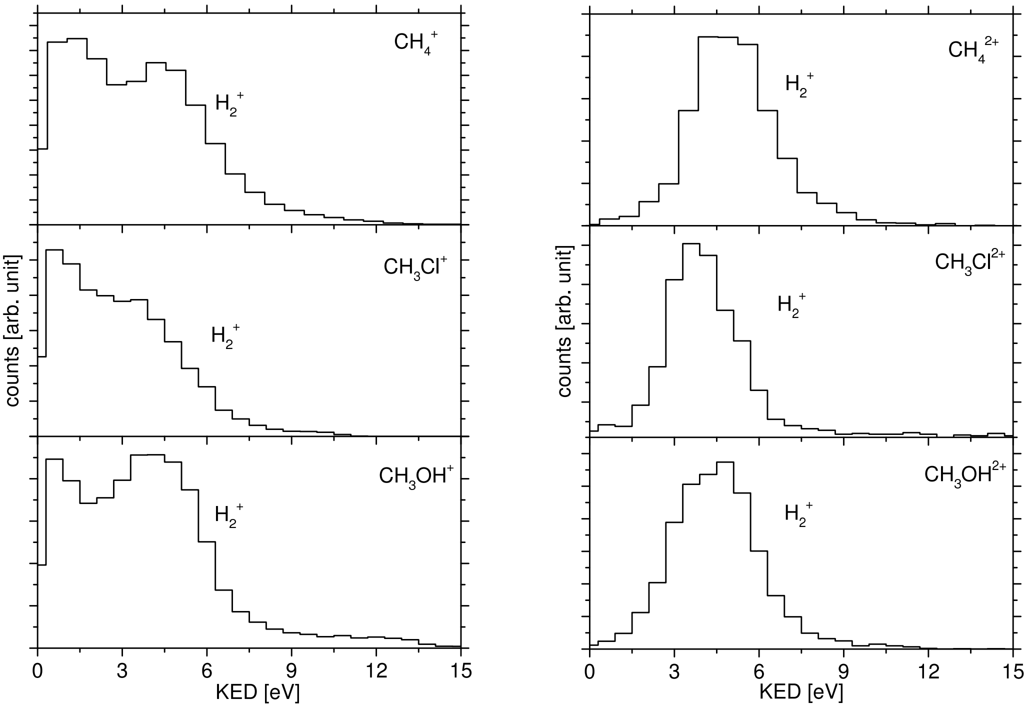

Figure 4.3: **[left]** Kinetic energy distribution of H_2^+ ions ejected from singly ionized precursor **[right]** Kinetic energy distribution of H_2^+ ions ejected from doubly ionized precursor.

the association between the hydroxyl H and methyl H atom. The KED profile of H_2^+ ion ejected from doubly ionized precursor is single peak at higher energy which means that most of the dissociative channels are arises from same excitation energy of doubly ionized precursor.

The similarity in the KED profiles of H_2^+ from different singly ionized precursors suggests that the functional group (–Cl or –OH) does not affect the kinematics substantially, but only play a role in enhancing the association. The kinematics seem to be governed more by the CH_3 group while the –Cl or –OH groups contribute to the distortion.

In all KED profiles of ions from doubly charged precursors, there is a possibility that the profile may be populated due to the ejection of H_2^+ from doubly ionized precursor in which the other fragments are not detected by detector due to less coincidence detection efficiency. Observed coincidence map and unique KED profile of associative fragments ejected from the doubly ionized precursor indicates that the contribution from doubly ionized precursor may be very small in the KED profile of H_2^+ ion of singly ionized precursor.

Kinetic energy distribution of H_3^+

The observed kinetic energy distribution of H_3^+ ion from singly and doubly ionized precursor of CH3Cl and CH3OH is shown in Figure 4.4. It is clear that the KED of H_3^+ ion from singly ionized CH3Cl and CH3OH is the double peaked structure. Since H_3^+ ion can originate only from methyl group of CH3Cl, the KE of this ion give us the group specific nature of kinetic energy distribution. By the comparing the KED of H_3^+ ion ejected from singly ionized CH3Cl and CH3OH, we conclude that the formation of H_3^+ ion from methyl group is occurred at higher excited state of precursor and the formation of this ion by migration and association between H atoms of both chemical group is arises from lower excited state of precursor.

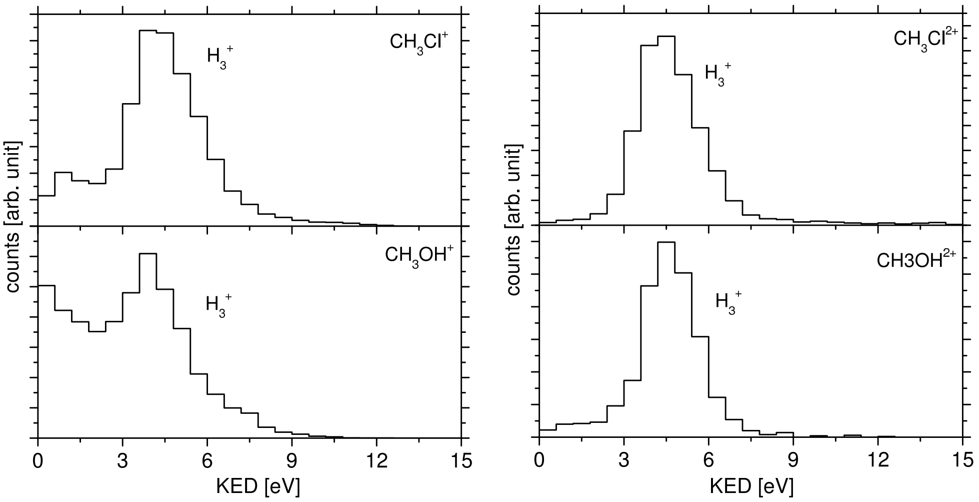

Figure 4.4: **[left]** Kinetic energy distribution of H_3^+ ions ejected from singly ionized precursor **[right]** Kinetic energy distribution of H_3^+ ions ejected from doubly ionized precursor.

The KED profile of H_3^+ ion ejected from doubly ionized precursor is singly peak profile at 4.5 eV. This suggests that the group-specific signature in the KED of H_3^+ is suppressed. In other words, it is not possible to say whether this profile is due to the formation of H_3^+ ion from methyl group alone or due to H atoms from both groups.

4.3 Site dependent bond association

In methanol, there are two chemical groups, methyl group and hydroxyl group, both of them having H atoms as their constituents. The formation of H_2^+, H_3^+ ions can occur from the association of H atoms in methyl group alone, or across the groups [Ruh90, Kus08]. Investigation of probability of formation of these ions from both chemical group requires differentiation between the H atoms of methyl group and H atom of hydroxyl group. This is possible by isotopic substitution of specific H atom sites. Isotopic substitution does not affect the chemical properties (except some minor deviations), hence the fragmentation patterns will be identical.

We have two possibility of differentiate the H atoms of both group, one possibility is CH_3OD molecule in which the H or D can easily identify that they are ejected from two different group, But there is ambiguity in distinguishing the H_2^+ and D^+ in the mass spectrum. Similarly, we cannot differentiate between DH^+ and H_3^+ ion due to same m/q ratio. Thus, we have used other option which is CD_3OH in which we can identify the site of each associative product. The relative yield analysis of associative product originating from singly and doubly ionized CD_3OH have been done for site specific probability of these ions.

4.3.1 Site-specific association probability

A partial mass spectrum of the fragments involving H or D ions (and their combinations) arising from dissociative ionization of CD_3OH and CH_3OH

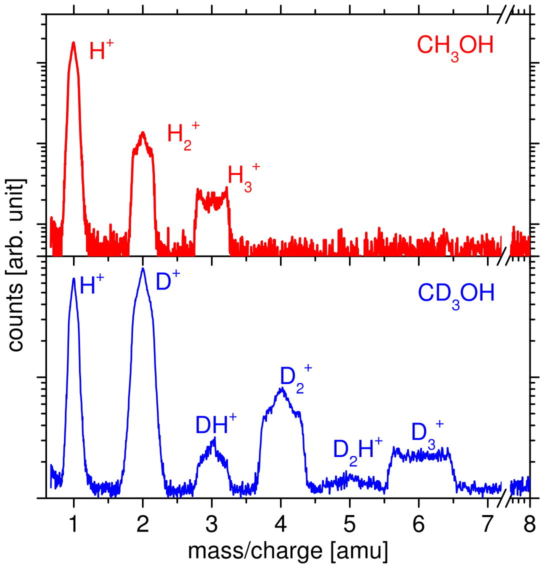

Figure 4.5: A partial mass spectrum of CH_3OH and CD_3OH by 1300 eV electron impact. It is noted that the profile of both peaks are not same. The counts under the peaks depends on their formation probability.

is shown in Figure 4.5. In the CD_3OH spectrum we observe ions of type $D_mH_n^+$ $(1 \leq m+n \leq 3)$. We focus our attention on them, as they point to migration and association of H or D atoms between the C and O sites. Normalization of the yield of each channel is carried as follows. Denoting the area under the peak by I, the spectra are normalized in a such a way that

$$\sum_{m=0}^{3}\sum_{n=0}^{1} I(\mathrm{D}_m\,\mathrm{H}_n^+) = 1 \qquad [1 \leq m+n \leq 3] \tag{4.1}$$

Due to the mass differences in the isotopes at the C and O sites, the sites involved in the formation of the ions can be uniquely identified and the probability of formation of each ion can be easily determined. On the other hand, the charge state of their precursors cannot be easily determined, since the singly ionized precursor as well as the doubly ionized precursor can yields singly charged fragments. However, contribution to a given ion species due to break-up of the dication can be identified via the ion-pair coincidence technique. The contribution to the total yield of a specific ion due to doubly charged precursors can then subtracted, giving us the contribution from singly charged precursors. Table 4.2 shows the relative probabilities for the formation of all ions of type $D_mH_n^+$ from singly and doubly

Table 4.2: Relative probabilities of formation of $D_mH_n^+$ ions from singly and doubly ionized precursors. Normalization is given by equation 4.1. The error in the determination of the probabilities is 2% for H^+ and D^+ increases to 25% for D_2H^+.

precursor	H^+	D^+	DH^+	D_2^+	D_2H^+	D_3^+
CD_3OH^+	0.308	0.476	0.013	0.055	0.004	0.015
CD_3OH^{2+}	0.043	0.065	0.003	0.012	0.001	0.005
Total	0.351	0.541	0.016	0.067	0.005	0.020

ionized precursors.

Noting that there are three D–C bonds in the molecule, we conclude that the breaking of a given D–C bond in CD_3OH (or, equivalently the H–C bond in CH_3OH) is half as likely as the breaking of the O–H bond. We further find that the D_2^+ ion is formed dominantly by association of the atoms in the methyl group. Migration of an H atom from the hydroxyl group followed by association with the atoms in the methyl group is approximately one-fifth as likely. The pattern repeats itself in the rearrangements leading to the formation of D_3^+ (or D_2H^+).

4.3.2 Kinetic Energy of associative ions

All associative fragments ejected from ionized CD_3OH precursor are site specifically known. For example, the ejection of D_2^+ or D_3^+ ions can be only from the methyl group. Similarly, the ejection of DH^+ or D_2H^+ ion is possible only when the migration and association occur in both chemical group. Since the processes are different for ejection of these ion, the kinetic energy of associative fragments ejected from various dissociative channels of singly and doubly precursor may differ, depending on the excited state and the association and migration aspect. The kinetic energy distribution of all associative fragments ejected from singly and doubly ionized CD_3OH precursor

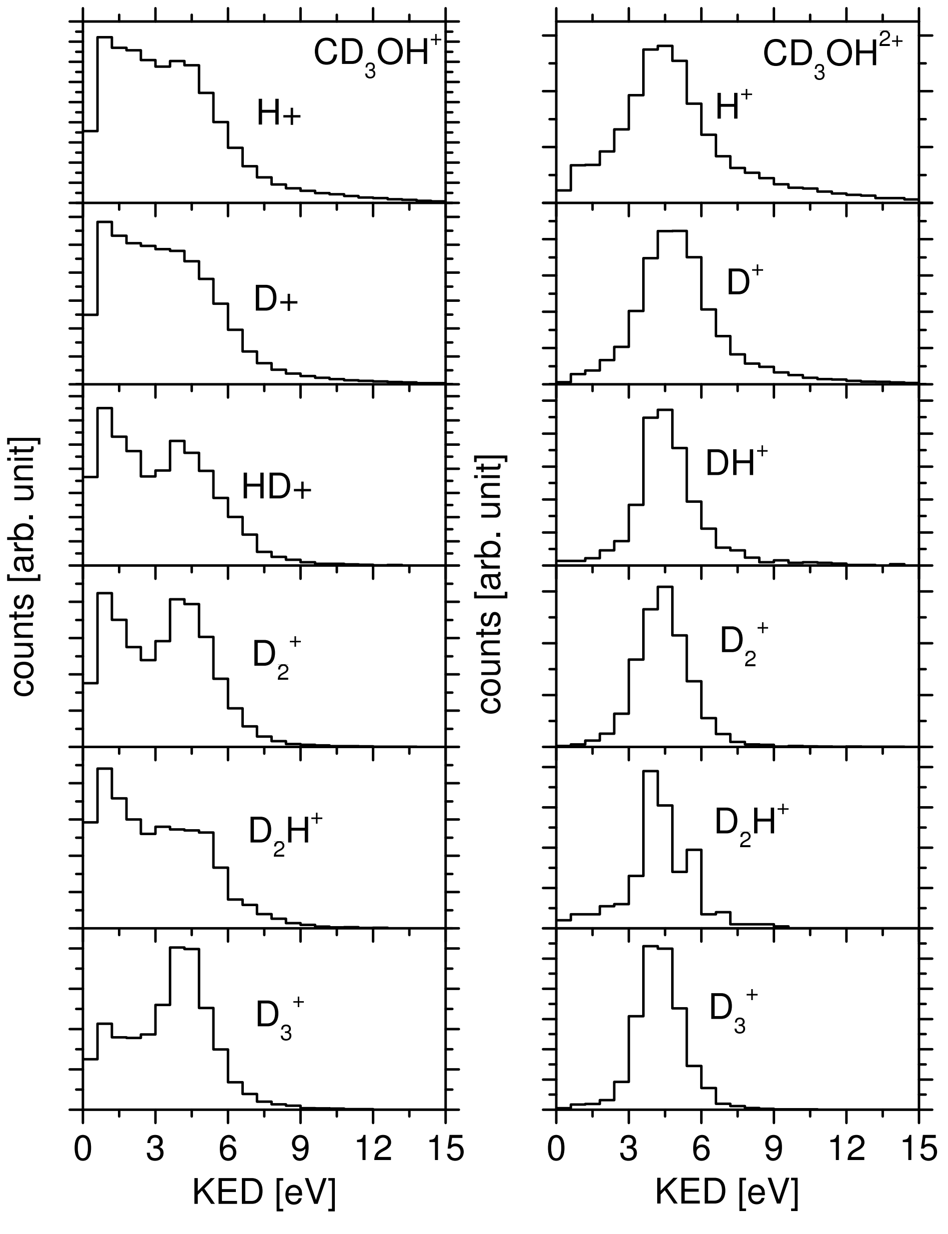

Figure 4.6: **[left]** Kinetic energy distribution of $D_mH_n^+$ ions ejected from CD_3OH^+, **[right]** Kinetic energy distribution of $D_mH_n^+$ ions ejected from CD_3OH^{2+}

is shown in Figure 4.6. The ejection of H^+ or D^+ is due to bond break-up process.

The KED profile of $D_mH_n^+$ ions are superposition of two distinct profile peaked at low (1.0 eV) and high (4.0 eV). In case of D_2^+ or D_3^+ KED , the low energy peaked profile is suppressed and most of the counts are appears in high energy peaked profile which is consistent with our previous result on CH_3Cl and CH_3OH. It means that the high energy peak is correspond to those associative ion which are ejected from the methyl group alone. It is noted that the low energy peak is also well resolved, which indicates the possibility of another molecular state of the methyl group. The KED of DH^+ or D_2H^+ ions profile is also double peaked but in this case the higher energy peak are suppressed. This indicates that the major production of associative ion occurs by migration and association of H atoms of both group is prominent at low energy molecular state of precursor. On the basis of these KED profile, we conclude that the D_2^+ or D_3^+ ions originate from higher excited states of singly ionized precursor compared to the formation of DH^+ or D_2H^+ which originate mainly from low excited state of precursor ion.

The KED of associative fragments of doubly ionized precursor are single profile peaked at 4.0 eV. It means that at higher energy, atoms on all sites in molecular ions are equivalent for association and migration. Due to this, the nature of site-specific association disappears in KED profile of associative ions arising from doubly ionized precursor.

4.4 Conclusions

We have performed a detailed investigation of atom-atom association in various fragmenting molecular ions. We have found that the association process occurs even in linear triatomic molecules, with the ejection of the central atom and formation of a bond between the terminal atoms. We conclude that this is only possible if the molecular ion is sufficiently bent to initiate association between terminal atoms prior to dissociation. This idea of *distorted geometry* is further explored in association process in a tetrahedral symmetric molecule, CH_4. In this molecule the mechanism of H_2^+ ion formation is studied. To strengthen the distortion hypothesis, we investigated the association process in dissociative ionization of molecules which have distorted tetrahedral structures in the neutral state. For this, methyl derivatives such as CH_3Cl and CH_3OH were chosen. Due to the high electronegativity of the substitute radical (–Cl or –OH), the association pattern is found to be different than the CH_4. In both cases the electronegative radical is found to initiate the formation of H_3^+ ion. This study of associative fragments indicates ways of formation of rare radicals such as H_3^+ by methods other than many-body recombination, which could be of significance in environments such as planetary and stellar atmospheres.

We have also conducted a detailed investigation of the process involving H atom migration and bond association in the fragmentation of methanol dications within and across the methyl and hydroxyl groups. To enable easy identification of the dissociation channels and the dissociation sites, the isotopomer CD_3OH was used for the experiment, instead of CH_3OH. Several dissociation channels in which the fragment ions formed by association of H atoms in methanol have been identified and the probability of their formation from the methyl and hydroxyl sites is obtained. Our analysis shows that during the dissociation of the methyl dication, the probability of association of the H atoms on the methyl site alone is nearly four times as large as the probability that the H atom on the hydroxyl site migrates and associates with the H atoms on the methyl site. Structures in the kinetic energy distributions of the associative fragments can be attributed to the role of various functional groups and large scale distortions in the molecular ions leading to the formation of new bonds and the subsequent ejection of associative fragments.

Chapter 5

Multi-atom Migration and Association

In small triatomic molecules such as H_2O, CS_2 or in tetrahedral symmetric molecules such as CH_4, CH_3Cl, association occurs between the nearest neighbor atoms. Formation of H_2^+ from ionized H_2O is an example of two atom association, as is H_2^+ and HCl^+ formation from ionized CH_3Cl. Further, H_3^+ ion formation from CH_3Cl is an example of three-atom association between neighbors. In polyatomic hydrocarbon molecules, such as in CH_3OH, migration of one or more atom may compete with nearest neighbors in the association process. To the best of our knowledge, there are no reports of associative reactions involving more than 3 atoms. As seen in the previous chapter CH_3OH which has two chemical groups, methyl and hydroxyl, exhibits migration of H atoms, as shown by the formation of OH_2^+ from ionized CH_3OH. We now explore the possibility of multi-atom migration and association. For this we first look into migration and association processes in the fragmenting CH_3CH_2OH molecule and then compare the associative processes in two structurally very similar molecules acetone (CH_3COCH_3) and dimethyl sulfoxide (CH_3SOCH_3).

5.1 Atom migration in fragmenting ethanol dication

To investigate the migration of H atoms across functional groups in case of ethanol, it is important to distinguish between H atoms on the C sites (CH_3– and CH_2–) and the O site. The methyl group (CH_3) is well separated ($\sim$ 3 Å) from the hydroxyl group, so we assume that migration of H atom from this group to O-site to be unlikely, and difficult to measure experimentally. But the migration of H atom from C-site of CH_2- to the O-site is quite possible, and may produce the OH_2^+ or OH_3^+ ions. Recently, De et al have reported the association between H atom of methyl group and H atom of hydroxyl group in alcohol induce by ion impact [De06]. Several groups have attempted to investigate the fragmentation processes in alcohol induced by intense laser field [Raj03, Kri04, Fur05]. Recently, our group has determined the site-specific probability for intra-molecular bond rearrangement in dissociative ionization of CH_3CH_2OH [Sha06] by electron impact and has reported that H_3^+ preferentially formed by rearrangement of H atom of Hydroxyl and CH_2 site than by association involving CH_3 site along. Our investigation is focussed on the migration of H atom in ethanol induced by electron impact. To ensure that we can identify that only H atoms from the CH_2– site have migrated to form the above mentioned ions, we use the isotopically substituted molecule CH_3CH_2OD for our study.

5.1.1 Formation of ODH_n^+ (n=1,2)

The evidence of atom migration and associative dissociation appears in some of the dissociation channels. The evidence for the formation of ODH_n^+ type of ions is very weak in the TOF spectrum of the first ion (hit1), because it might be merged with the background. It is however seen in the ion–ion coincidence map of CH_3CH_2OD shown in Figure 5.1. The ODH^+ and ODH_2^+ ions are detected in coincidence with CH_3C^+ ion. It is clear

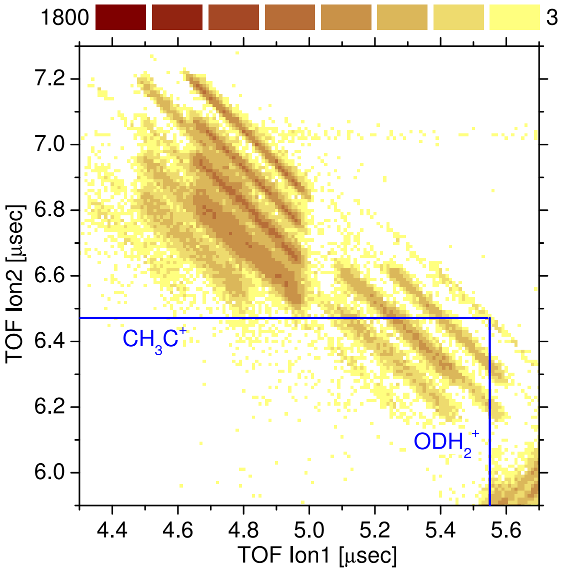

Figure 5.1: Partial ion-ion coincidence map of CH_3CH_2OD. The islands appears in this map are the representative of various dissociative channels of $CH_3CH_2OD^{2+}$.

that these ions are originated from -CH_2OD site of molecule. Intensity in the ODH_2^+:CH_3C^+ island is low compared to all other island which tell us the less probability of two H atom migration which led to the formation of ODH_2^+. The details about the kinematics of ODH_2^+ and ODH^+ ejection is discussed in the next sections.

5.1.2 Kinematics of ODH_2^+ ejection from $C_2H_5OD^{2+}$

The formation of ODH_2^+ ion is an evidence for two H atom migration from the -CH_2 site to the O-site followed by association. The slope of the coincidence island is close to -1, so the formation of ODH_2^+ ion is via a two-body break-up. The reaction for ODH_2^+ formation is

$$CH_3CH_2OD^{2+} \longrightarrow ODH_2^+ + CH_3C^{2+} \tag{5.1}$$

For kinematic study of this fragments, we have measured the momentum of both fragments. We have found that the momentum profile of both fragments are same. The observed momentum of fragments have been used to calculate the kinetic energy of each fragments and thus we can obtain the kinetic energy release. The kinetic energy release distribution provides information regarding the molecular states contributing to a dissociation

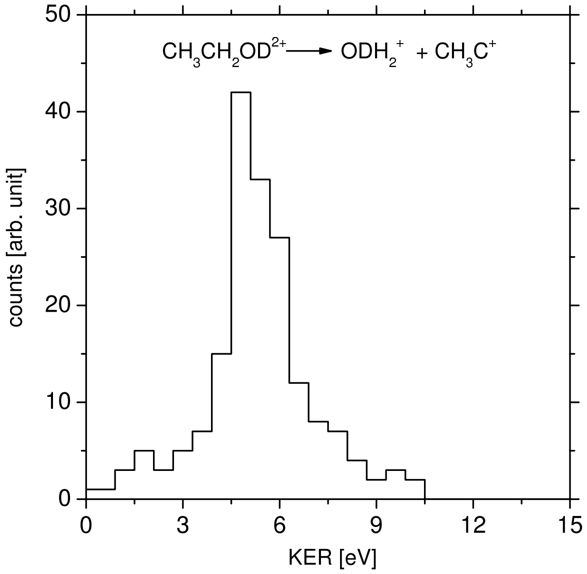

Figure 5.2: Kinetic energy release for the ODH_2^+ ion formation in two-body break-up from dication C_2H_5OD. The KER is sum of KE of ODH_2^+ and KE of CH_3C^+.

reaction, the most probable KER values are used to characterize the excited molecular states leading to prominent dissociation channels. The large structural changes during migration of atom in precursor ion may have various molecular excited states. The evidence of molecular states and structural changes in precursor ion may be appeared in KER distribution. The kinetic energy release (KER) for ODH_2^+ ion formation in two-body break-up is shown in Figure 5.2. The multi peaks profile of KER indicate more than one repulsive molecular states of precursor. The peak values of KER are 1.2, 4.8 and 9.6 respectively. The prominent peak is at energy 4.8 eV which means that most of the two-atom migration occurs at this energy of repulsive molecular excited state where major structural change in precursor is possible which led to the formation of ODH_2^+ ion.

5.1.3 Kinematics of ODH^+ ejection from $C_2H_5OD^{2+}$

The intensity of ODH^+:CH_3C^+ island is more compared to the ODH_2^+:CH_3C^+ island which indicates that the formation of ODH^+ ion is more probable than the formation of ODH_2^+ ion. The ODH^+ ion formation is an evidence of one H atom migration from the -CH_2 site to the O-site followed by association. The formation of this ion occurred in three-body break-up of pre-

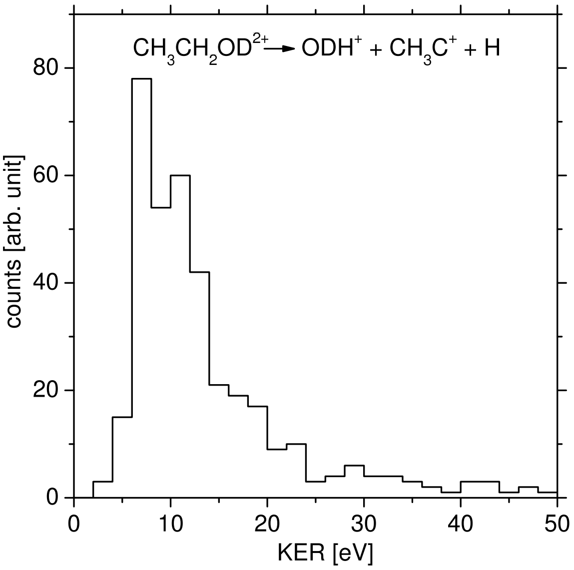

Figure 5.3: Kinetic energy release for the ODH^+ ion formation in three-body break-up from dication C_2H_5OD.

cursor. The reaction for ODH^+ ion production is

$$CH_3CH_2OD^{2+} \longrightarrow ODH^+ + CH_3C^{2+} + H \tag{5.2}$$

Our aim is to understand the ejection kinematics and the formation mechanism of ODH^+ ion in three-body break-up. Detection of this ion in coincidence with CH_3C^+ ion supports the hypothesis that H atoms of methyl group are not participating in association or not migrating to other sites. The D and two H atom of –CH_2OD are involved in migration and association. Neutral H is also ejected during the formation of ODH^+ ion. Mapping the ejection of neutral H, ODH^+ ion and CH_3C^+ ion can tell us whether the migration of H atom of –CH_2- site to the O-site occurs in sequential or concerted process. For this purpose, we have constructed the momentum map from observed momentum vector of both charged fragments and the neutral. It is noted that the momentum of neutral is calculated on the basis of momentum conservation in three-body break-up. The momentum map for ejection of ODH^+ ion from the dication C_2H_5OD is shown in Figure 5.4. It is clear from the momentum map that the magnitude of momentum of ODH^+ and CH_3C^+ ion are same which indicates the two-body break-up of precursor. Neutral H is ejected in first stage of break-up. Thus, we con-

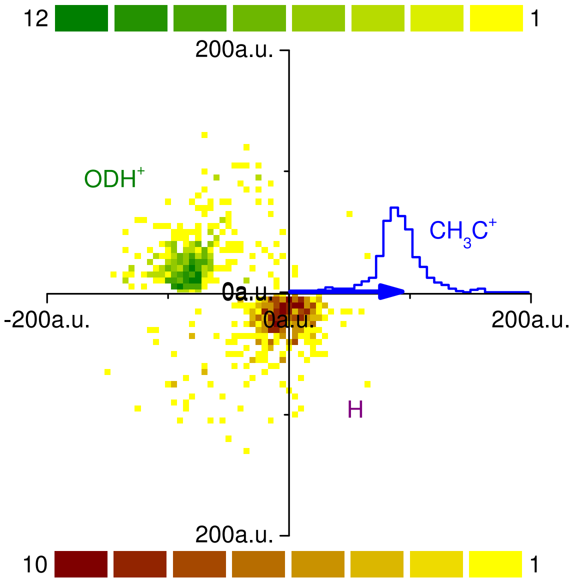

Figure 5.4: Momentum map for ODH$^+$ formation in three-body break-up of $CH_3CH_2OD^{2+}$. Ejection of CH_3C^+ ion taken as reference (x-axis), longitudinal and transverse momentum components of other fragments are plotted. Momentum distribution of CH_3C^+ is also shown.

clude that the ODH$^+$ ion has originated via sequential break-up of dication C_2H_5OD.

The observed momentum of all fragments have been used to calculate the kinetic energy of each fragments and thus we have obtained the KE distribution for ejection of ODH$^+$ ion in three-body break-up. It is assumed that the structural changes in precursor and migration of one H atom from C-site of –CH_2- site to the O-site occurred simultaneously for a given excited molecular state. The evidence of molecular states can be appeared in KED distribution. The observed KER distribution for ODH$^+$ ion ejection in three-body break-up reaction is shown in Figure 5.3. It is clear that the single H atom migration occurred at higher excited molecular state of precursor.

5.2 Atom migration in fragmenting acetone and dimethyl sulfoxide dication

In the previous section, we have investigated the migration of H atom in fragmenting C_2H_5OD dication. We have found the formation of ODH$^+$ and ODH$_2^+$ ion from the unique dissociative channels. As we realized that the

ODH_2^+ ion formation is the result of two H atom of –CH_2- site migrating to O-site and association. Similarly, the ODH^+ formation is the result of one H atom of C-site migrated to O-site. In ethanol we have observed the evidence of migration of atom and association process during fragmenting of precursor ion. For more than two atom migration, the fragmentation of ionized acetone (CH_3COCH_3) and dimethyl sulfoxide (CH_3SOCH_3) molecule have been investigated. Dimethyl sulfoxide is geometrically different molecule compared to acetone. The association reactions of both ionized molecules are compared to estimate the role of geometry in atom migration and association reaction. The details about the ground state geometry is discussed in next section.

5.2.1 Geometry of CH_3COCH_3 and CH_3SOCH_3

The ground state geometry of these molecules is shown in Figure 5.5 and It is noted that the methyl group in both molecule is same. The only difference in geometry is the C–C–C chain and O in acetone are in plane on the other hand the C–S–C chain and O in dimethyl sulfoxide are not in a single plane. The distance between both methyl group in acetone is large compared to dimethyl sulfoxide. The bond angle and bond strength of CH_3COCH_3 and CH_3SOCH_3 molecules are given in Table 5.1 [Sve74, Kuc98]. It is clear from the experimental data of geometrical parameters that the geometry of the

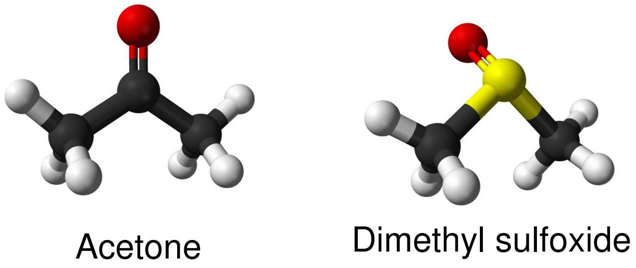

Figure 5.5: **[left]** The ground state geometry of acetone. **[right]** The ground state geometry of dimethyl sulfoxide

Table 5.1: Geometrical parameter of CH_3COCH_3 and CH_3SOCH_3 (distances (r) in Å, angles (a) in degrees)

CH_3COCH_3	CH_3SOCH_3
rCO = 1.215	rSO = 1.485
rCC = 1.515	rCC = 1.515
rCH = 1.086	rCH = 1.093
aCCC = 116.4	aCSC = 96.6
aHCC = 110.3	aHCS = 109.6
aCCO = 121.8	aCSO = 106.5

two molecules are slightly different even though they have similar molecular formulas or functional groups. Due to geometrical difference, the bond association processes in dimethyl sulfoxide and acetone will differ. We look for ions that carry the signature of multi H atom migration in these molecules.

5.2.2 Formation of OH_n^+ (n=2,3) from fragmentation of dication acetone and dimethyl sulfoxide

The observed ion-ion coincidence map of CH_3COCH_3 and CH_3SOCH_3 is shown in figure 5.6. Some of these channels are due to the bond association and bond break-up reaction. The example of the association reactions are the formation of H_3^+, H_2^+ ions via various dissociative channels. These ions are originated from methyl group.

Formation of OH_3^+ and OH_2^+ ions are seen in the coincidence map of CH_3SOCH_3. It is noted that the formation of these ion are possible only when the migration of H atoms from any of the C-sites (methyl group) to the O-site takes place. The formation of OH_3^+ ion is the evidence of three-atom migration and association process. It is noted that formation of OH_3^+ ion is not detected in the coincidence map of CH_3COCH_3. It means that the large

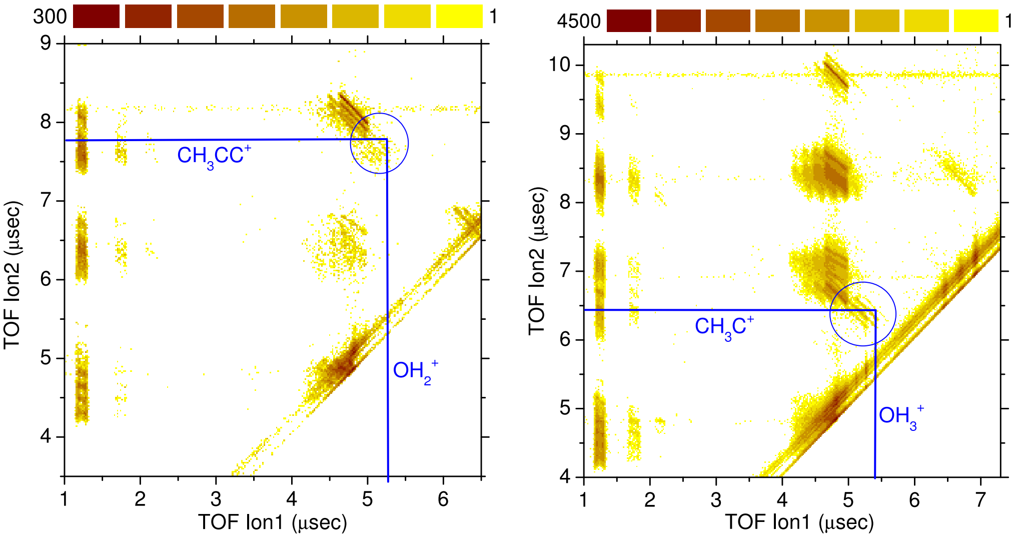

Figure 5.6: **[left]** Ion-ion coincidence map of fragments from $CH_3COCH_3^{2+}$. **[right]** Ion-ion coincidence map of fragments from $CH_3SOCH_3^{2+}$

geometrical deformation of $CH_3SOCH_3^{2+}$ ion have suitable molecular states which initiated the three H atom migration from methyl group to O-site. In CH_3COCH_3, due to long distance between the H atoms of methyl group and O-site three H atom migration is unlikely. Formation of OH_2^+ ion is found in coincidence with CH_3CC^+ ion in coincidence map of acetone with very less counts. This is the evidence of two-atom migration. The details about the two-atom migration reaction is already discussed in the previous section. In this section, we focus on the three-atom migration phenomena. The major issue is to know the types of process which initiate the three-atom migration. The ejection mechanism of OH_3^+ ion is discussed in the next section.

5.2.3 Ejection mechanism of OH_3^+ from $CH_3SOCH_3^{2+}$

Formation of OH_3^+ ion is the result of three atoms migration and association. This is a special reaction which needs to be investigated further. The cross-section of this ion formation is very small compared to the formation of any

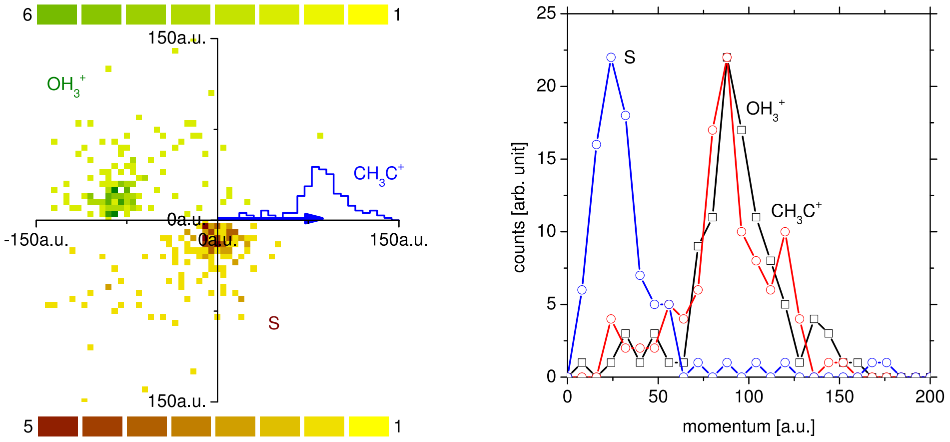

Figure 5.7: Momentum map for ejection of OH_3^+ ion from $CH_3SOCH_3^{2+}$ in three-body break-up reaction.

other fragments via any dissociative channels. The three atom migration in any molecule is a rare process. The multiple atom migration depends on the various parameters such as the geometry of molecules, availability of high electronegativity site and favorable perturbation. The most important parameter is the large structural changes in molecular ion during dissociative ionization. The formation of OH_3^+ ion occurs due to large structural changes in precursor ion. Since OH_3^+ ion is ejected in three-body break-up, the type of reaction such as the sequential or concerted through which this ion is ejected is not known. The island through which this ion is observed is OH_3^+:CH_3C^+, which indicates that third fragment must be either S or S^+. Since S^+ ion is not detected in the third hit spectra which indicate that the third fragment is neutral S atom. It is noted that the S atom is present in the center of CH_3SOCH_3 molecule and is strongly attached to two C atoms. The prediction about the geometrical deformation is difficult due to complex geometrical structure of ground state and possibility of various dissociative state in ionized state. Some of the dissociative state may initiate the multi H atom migration. During the migration of H atoms, the S atom is expected to be present in precursor but the detection of OH_3^+ ion in coincidence with CH_3C^+ ion indicates that the S is ejected during fragmentation. It means that both C–S bonds break during migration process. On the basis of geometry, it is clear that the sequential break-up of precursor in which S is ejected in the first stage of break-up, is not possible. We can explore the ejection pattern of all fragments. The details about the type of reaction and ejection pattern can be visualize in momentum map. To construct the momentum map, we have calculated the momentum of neutral S by momentum conservation. The momentum map for ejection of OH_3^+ ion via three-body reaction is shown in left panel of Figure 5.7. It is clear from the momentum map that most of the momentum is taken by charged fragments such as OH_3^+ and CH_3C^+ ions which seem to be back-to-back ejection. This result indicates two possibility, one is the concerted break-up of precursor in which the neutral S atom carry very less momentum. Other possibility is the sequential ejection of S in first stage of break-up and OH_3^+ ion is formed from second stage of break-up. By comparing the momentum of S with momentum of charged fragments, we can draw some conclusions. The momentum of all fragments are also shown in right panel of Figure 5.7. It is clear that the neutral S carry one-fourth of charged fragments momentum. This is a strong evidence which tell us that the OH_3^+ ejection occurrs in concerted break-up of $CH_3SOCH_3^{2+}$ ion. The possible dissociative reaction for this ion production is written as

$$CH_3SOCH_3^{2+} \quad \longrightarrow \quad OH_3^+ + S + CH_3C^+ \tag{5.3}$$

It is noted that the migration of all three H atoms of any one methyl group to O-site or any three H atom from both methyl group is possible. The both chemical groups are equivalent in this molecule, the process of H atom migration from any or both methyl group to O-site may have equal probability.

5.3 Conclusions

We have investigated the multi-atom migration and bond association in various polyatomic hydrocarbon molecules such as ethanol, acetone and dimethyl sulfoxide. In d-ethanol, we have found evidence of two H atom migration. Two atom migration and formation of ODH_2^+ ion from C_2H_5OD dication occurs in a two-body reaction from the $–CH_2OD$ portion of the molecule.

In investigating the role of small geometrical differences between two structurally similar molecules such as CH_3COCH_3 and CH_3SOCH_3 and the possibility of more than two atom migration, we have found evidence of three atom migration and formation of OH_3^+ ion from fragmenting CH_3SOCH_3 dication. The formation of OH_3^+ ion is not observed in the case of the CH_3COCH_3 dication, which points to an important role of geometry in multi-atom migration. Due to the lone pair of electrons at S, the O atom is not in the C–S–C plane but and is closer to the H atoms of methyl group (than in the case of acetone). This might be the one of the reason that the OH_3^+ ion is found in fragmenting CH_3SOCH_3 dication but not found in fragmenting CH_3COCH_3 dication. We have done detailed momentum map analysis for investigation of break-up pattern of the precursor and formation of this ion. We have found that the OH_3^+ ion is ejected in concerted three-body break-up process.

Chapter 6

Geometry of Unstable Molecular Ions

Different kinds of spectroscopic techniques, for example IR, Microwave and Raman spectroscopy, can give information about the molecular geometry from the details of the vibrational and rotational absorbances. These conventional spectroscopic techniques have been well established for obtaining the geometrical properties of neutral molecule. Owing to their instability, these techniques cannot be applied to molecular ions. Estimation of the geometry of unstable molecular ion by experiment is most challenging task due to its short life time. Recently, attempts been made to map the geometry of molecular ion by fragment momenta measurement in three or more body break-up reaction [His99, Bry00, Bap07]. Geometrical deformation and its effect on the bond association process are the key interest of this thesis. In this chapter, we describe two methods of estimating some geometry parameters of the molecular ion, in context of three-body fragmentation of doubly and triply ionized molecules.

6.1 Kinematics of three-body fragmentation

In fragmentation dynamics of molecules, the investigation of three-body break-up reaction can give more information about the precursor than the two-body break-up. We know that in two-body break-up, the fragments are ejected back-to-back from which we can not extract geometrical information about the precursor. In three-body break-up, the kinematic information of fragments can be used to estimate the dissociative geometry of precursor ion. It is noted that the kinematic information can be used only for those precursors which are fragmenting via three- or many-body simultaneous break-up. The details about the simultaneous and sequential break-up of precursors have already been discussed in chapter 3.

The singly ionized molecular ions are often stable but the doubly, triply or higher ionized molecular ions are mostly unstable and dissociate into two or many fragments. If singly ionized molecular ion dissociate via three-body break-up, only one charged fragments are detected by present set-up and neutral fragments are not detected. In this case, complete kinematic information of all fragments are not available. Thus, we are unable to map three-body break-up of singly ionized precursor. In case of three-body break-up of doubly ionized precursor involving separation of charges, at least two charged fragments are detected by spectrometer and kinematic information (such as momentum) of both fragment are measured. In simultaneous or concerted three-body break-up of precursor, the momentum of neutral fragment can be obtained by momentum conservation. Thus, for such reaction we have kinematic information of all fragments. The momentum spectrometer is very powerful for mapping the such kind of three-body reaction. In fact, this technique is very much useful for mapping the complete three-body Coulomb explosion which eject all charged fragments. The present spectrometer can be used to map the many-body fragmentation of molecular ion but our aim is focused on the association processes in fragmenting molecular ion. We have investigated the association processes in doubly and triply ionized precursor. Thus we will be confined to study the kinematics of three-body fragmentation of these precursor. As seen in the previous chapter, the association yield depend on the geometrical deformation of molecular ion. The kinematic information of all fragments in simultaneous three-body break-up can be used to map the dissociative geometry of precursor ion. It is noted that the momentum imaging method estimate the geometry of molecular ion at the time of break-up. The geometry of molecular ion at the time of break-up is not same as the ground state geometry.

In three-body break-up of doubly ionized precursor, the Coulomb force affects only the charged fragments, while the neutral momentum remains unaffected. On the other hand, in three-body Coulomb explosion the trajectory of each fragment is affected by the Coulomb effect. Thus the angles between the momentum vectors measured by momentum imaging are not the actual angles in the molecular ion. For actual geometry of dissociating ion, a classical trajectory simulation is necessary to estimate the Coulomb effect on the trajectory of fragments.

Our results of association and migration of atom in fragmenting molecular ions demand mapping of various precursor ion. For mapping the geometry of doubly ionized precursor, we have chosen the doubly ionized CH_3Cl precursor, in which an associative channel leading to the formation of H_2^+ is observed. Further, for the case of three-body Coulomb explosion, we have chosen the case of triple ionization of CO_2 by soft x-ray absorption. The latter experiment was done by us at the Indus-1 synchrotron using an apparatus very similar to the one described in Chapter 2, a brief description of the experiment appears in the Appendix B.

6.2 Geometry of doubly ionized precursor

Let us consider concerted dissociation of $(ABC)^{2+}$ ion into three fragments.

$$(ABC)^{2+} \rightarrow A^{+} + B^{+} + C \tag{6.1}$$

A^{+}, B^{+} and C may be atomic or molecular fragments. In this reaction, the charged fragments A^{+} and B^{+} are detected by the spectrometer and momentum of these ions are measured. The momentum of neutral C can be obtained from the momentum conservation. Once we have momentum of all fragments, we can calculate the angle between any two fragments. For a given ejection direction (taken as a reference vector, along x-axis) of any ion, the angular distribution of other fragments with respect to the reference can be plotted as a polar plot. That plot may give the information about the ejection of fragments in three-body break-up of doubly ionized precursor. Same information can be used to map the geometry of fragmenting molecular ion.

We now focus on mapping the geometry of unstable doubly ionized methyl chloride (CH_3Cl^{2+}), which dissociates via a concerted break-up into three fragments and also contains an associative fragment. The fragmentation reaction is

$$CH_3Cl^{2+} \quad \longrightarrow \quad H + H_2^{+} + CCl^{+} \tag{6.2}$$

In this process, all fragments should be confined in one plane to conserve the momentum. Thus the geometry of the precursor must be planar. For further details about the dissociative geometry of these ion, the observed momentum of fragments have been used to obtain the angular distribution between any two fragments. The momentum of neutral fragments is obtained by conservation of momentum in three-body break-up. The polar plot is shown in the upper panel of Figure 6.1, and the proposed geometry on basis of polar plot for H_2^{+} ejection channels is shown in the bottom panel.

We propose a simple model to explain the angle between the asymptotic velocity vectors as shown in polar plot. In this model, the one component of the momentum vector of each of the two charged fragments is calculated

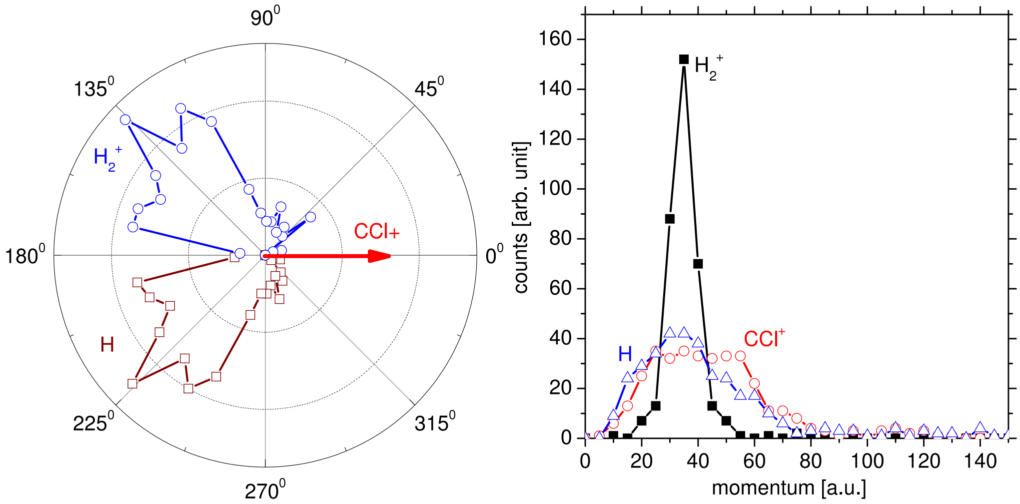

Figure 6.1: [left] Polar plot for three-body break-ups of CH_3Cl^{2+}. In this plot, the ejection direction of CCl^+ is taken as reference and the angular distribution of other fragments are plotted with respect to that. [right] observed momentum of all fragments.

from the KER under a Coulomb model and momentum conservation. The momentum of the neutral is taken to be the momentum component perpendicular to the direction of separation of the charges. The unknown variable is the initial separation R between the charged fragments.

In Coulomb model, the expression for KER (KER in eV and R in Å) is

$$\mathrm{KER} = 14.4\frac{q_1 q_2}{R} = \sum_{i=1,2} \frac{P_i^2}{2M_i} \tag{6.3}$$

where the q_1, q_2 are the charge on fragments and R is the inter-atomic distance at the time of explosion. The P_i is the momentum along the line of separation and M_i mass of i^{th} ions. Let us denote the momentum of H_2^+ by $\overrightarrow{P_1}$, mass M_1 and for CCl^+ ion, the momentum $\overrightarrow{P_2}$ and mass M_2. Momenta of the two fragments are back to back, hence

$$\overrightarrow{P}_1 = -\overrightarrow{P}_2 \tag{6.4}$$

By solving the equation 6.3 and equation 6.4, one can obtain the momentum of charged fragments along the line of separation, for a given R. In the molecular frame of reference, the two separating charge particles are not moving back to back, as the neutral momentum is not zero. The angle between the momentum vectors of charged fragments and the momentum of neutral fragment in the molecular frame within measured range can be used to explain the angular distribution between fragments in polar plot. The angle between the charged fragments in the molecular frame, denoted by α, is given by

$$\alpha = 2\tan^{-1}(\frac{P_i}{P_n}) \tag{6.5}$$

where P_i is the momentum of any charged fragments and P_n is the momentum of neutral. The momentum distributions of the three fragments determined measured in the experiment are displayed in Figure 6.1 (right panel). As we can see, the neutral momentum distribution is very broad. If we take the range as 10–60 a.u., the observed angular distribution of the charged fragments momentum vectors corresponds to an initial separation R between (2.5–0.4) Å, between H_2^+ and CCl^+. This range of R may be compared with the mean C–H separation of 1.06 Åand C–Cl separation of 1.72 Åin the neutral ground state [Her66, Dun73]. It is thus clear that the association is accompanied by substantial deformation in the precursor ion.

We have also mapped the geometry of CH_4^{2+} and CD_3OH^{2+} ion. The same method have been used to estimate the geometry of CD_3OH^{2+} which eject D_2^+ and DH^+ ions via three-body dissociative channels. On the basis of momentum map and kinetic energy release in these reaction, we have found that the geometry of intermediate CD_3OH^{2+} ion is deformed from the ground state geometry of CD_3OH molecule. Note that in a previous report [Bap07] bent states of CO_2^{2+} were proposed on the basis of the momentum distribution of the fragments, but that report did not take into account the effect of the neutral momentum on the angular distributions.

6.3 Geometry of triply ionized precursor

Since the electron impact experiment does not lead to triply charged molecular ions (the cross-sections at 1300 eV impact energy is too small), we have performed a photoionization experiment. This experiment have been performed at the Indus-1 Synchrotron Facility, Indore. 200 eV photon energy have been used to ionize the CO_2 molecule. Note, that photoionization follows selection rules, so the ionization process will be different from electron impact. However, we are primarily interested in establishing a method of arriving at the geometry of the triply charged precursor from the momentum distribution of the fragments, and not in the triple ionization mechanism. At 200 eV photon energy, the doubly as well as triply ionize precursor ions are formed. This energy is not resonant with any of the inner shells of C or O, so electron removal is mainly by valence shell ionization followed by shake-off [Amu92, Sai94, Yam06].

Triply charged CO_2 dissociates via four possible dissociative channels. The details about the dissociative channels of precursor ion is reported recently by our group [Sin06]. For the purpose of this study, we focus on the three body dissociation dynamics of CO_2^{3+}. The purpose of this section is to show the experimentally mapped geometry of CO_2^{3+} ion which undergo three-body Coulomb explosion. The Coulomb explosion reaction of CO_2^{3+} is

$$CO_2^{3+} \longrightarrow C^+ + O^+ + O^+ \tag{6.6}$$

The momentum of all charge fragments are measured and angle between any two fragment vectors have been obtained. To extract the geometrical information of CO_2^{3+}, we have converted these angular distribution in form of polar plot. The ejection direction of C^+ ion is taken as reference (x-axis) and angular distribution of both O^+ ion have been plotted with respect to the reference. The polar plot of product distribution is shown in Figure 6.2. In the polar plot it appears that the geometry of CO_2^{3+} is distorted from

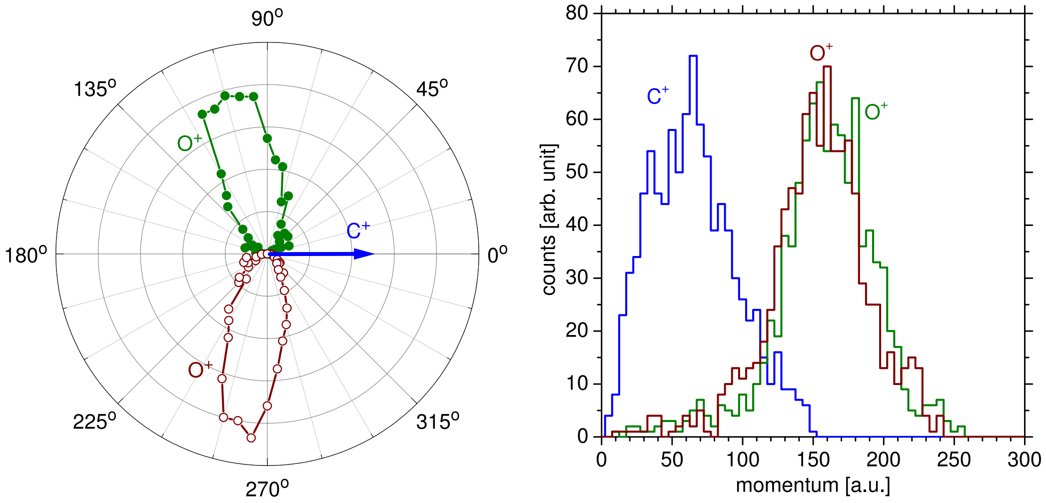

Figure 6.2: [left]Polar plot of ejected ions from Coulomb explosion of CO_2^{3+}. In this plot, the direction of ejection of C^+ is taken as the reference direction for each event. The angular distribution of O^+ ions w.r.t. the C^+ ions are plotted. [right] Observed momentum of all fragments.

linear geometry. However, the geometry apparent from the polar plot is not the actual geometry of the precursor due to the fact that the Coulomb repulsion affects the trajectories of the ions. To take into account the effect of Coulomb repulsion on the trajectory of charged fragments, we need the trajectory simulation. The classical trajectory simulation of fragments are discussed in the next section.

6.3.1 Trajectory simulation for three-body Coulomb explosion

In this section, we discuss the simulation of the trajectory of all fragments ejected from Coulomb explosion of CO_2^{3+} into C^+, O^+, O^+. All charge fragments have 1 unit of Coulomb charge. We assume that the explosion has occurred from bent state of CO_2^{3+}. We further assume that the trajectories of the two O^+ ions are symmetric w.r.t the trajectory of C^+. This assumption is wholly justified by the experimental data (See Figures 6.2). Note that the

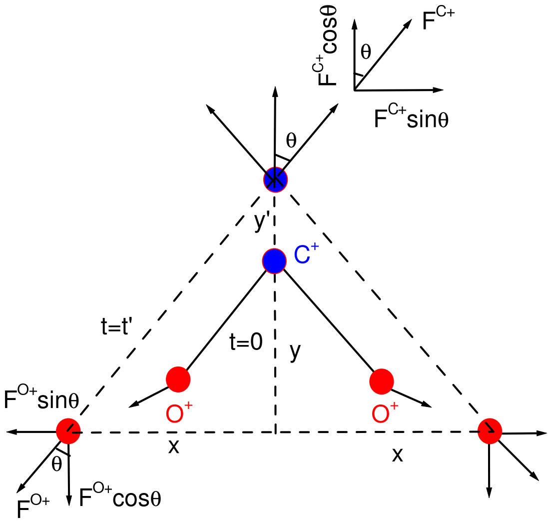

Figure 6.3: Schematic diagram of Coulomb explosion. The ejection of all charged fragments is shown in Figure. The initial state geometry is taken as bent. The geometry at $t = 0$ and the possible position of all fragments at $t = t'$ is shown. The components of forces on O^+ and on C^+ due to other charged fragments is also clearly shown.

momentum of C^+ is non-zero, which can only happen if the dissociation is from a bent state. Further, the momentum and angular distributions of the two O^+ ions are nearly identical.

The geometrical parameter for a given bent state will be used as a initial condition for solving the equation of motion of all fragments. The trajectory of O^+ is affected by repulsive Coulomb force due to C^+ and the other O^+. This forces will change the trajectory of any O^+. The horizontal component of Coulomb force on C^+ due to both O^+ is cancelled out, the only vertical component will push the C^+ ion. We can write down the classical equation of motion for calculating the trajectory of these fragments. Schematic diagram for ejection of all fragments from Coulomb explosion of CO_2^{3+} is shown in Figure 6.3. The equations of motion of C^+ and O^+ are derived below.

The force on C^+ due to both O^+ ions along y axis is given by,

$$\vec{F}^{C+} = \vec{F}_y^{C+}\hat{y} = 2\frac{1}{4\pi\varepsilon_0}\frac{e^2}{r^2}\cos\theta\hat{y} \tag{6.7}$$

$$\mathrm{m}_C \frac{d^2y}{dt^2} = 2\frac{1}{4\pi\varepsilon_0}\frac{e^2}{r^2}\frac{y+y'}{r} \tag{6.8}$$

Where $r = \sqrt{x^2+(y+y')^2}$

The force on each O^+ due to C^+ and other O^+ is given by

$$\overrightarrow{F}^{O+} = \overrightarrow{F}^{C^+}_{x}\hat{x} + \overrightarrow{F}^{O^+}_{y}\hat{y} \tag{6.9}$$

$$= \frac{1}{4\pi\varepsilon_0}\frac{e^2}{(2x)^2}\hat{x} + \frac{1}{4\pi\varepsilon_0}\frac{e^2}{x^2+(y+y')^2}\sin\theta\hat{x} + \frac{1}{4\pi\varepsilon_0}\frac{e^2}{x^2+(y+y)^2}\cos\theta\hat{y} \tag{6.10}$$

where the first term of R.H.S. is the force experienced by the O^+ ion due to other O^+ ion, and the next two terms represent, respectively, the x and y components of the force imparted by the C^+ ion.

$$= \frac{1}{4\pi\varepsilon_0}\frac{e^2}{(2x)^2}\hat{x} + \frac{1}{4\pi\varepsilon_0}\frac{e^2}{x^2+(y+y')^2}\frac{x}{\sqrt{x^2+(y+y')^2}}\hat{x} \tag{6.11}$$

$$+\frac{1}{4\pi\varepsilon_0}\frac{e^2}{r^2}\frac{y+y'}{\sqrt{x^2+(y+y')^2}}\hat{x} \tag{6.12}$$

Thus, the equations of motion of O^+ and C^+ ions are

$$\frac{d^2x}{dt^2} = \frac{e^2}{4\pi\varepsilon_0 m_O}\left(\frac{1}{(2x)^2} + \frac{x}{\sqrt[3]{x^2+(y+y')^2}}\right) \tag{6.13}$$

$$\frac{d^2y}{dt^2} = \frac{e^2}{4\pi\varepsilon_0 m_O}\frac{y+y'}{\sqrt[3]{x^2+(y+y')^2}} \tag{6.14}$$

and

$$\frac{d^2y'}{dt^2} = \frac{e^2}{2\pi\varepsilon_0 m_C}\frac{y+y'}{\sqrt[3]{x^2+(y+y')^2}} \tag{6.15}$$

Solutions of the above equations provide the effect of Coulomb repulsion on the trajectory of C^+ and O^+ ions. For solving the trajectory of O^+, we have two equations and three variables. By exploiting the symmetry in the problem one can transform all these above equations in form of two equations with two variables. In order to do so, we have to add or subtract equations and convert them into two equations. Adding the equation (6.14) to equation (6.15), thus, gives,

$$\frac{d^2(y+y')}{dt^2} = \frac{e^2}{4\pi\varepsilon_0} \frac{y+y'}{\sqrt[3]{x^2+(y+y')^2}} (\frac{1}{m_O} + \frac{2}{m_C}) \tag{6.16}$$

Let us introduce a new variable $z = y + y'$. Then,

$$\frac{d^2 z}{dt^2} = \frac{e^2}{4\pi\varepsilon_0} \frac{z}{\sqrt[3]{x^2+z^2}} (\frac{1}{m_O} + \frac{2}{m_C}) \tag{6.17}$$

Now we have two equations (6.13, 6.17) with two variables (x, z). To calculate the angle between the velocity vector, we have to calculate the velocity at t→ ∞ with given initial geometry which is a boundary value of above equation. From the Figure 6.3 the angle is defined as,

$$\tan\theta = \frac{\dot{x}}{\dot{y}} \tag{6.18}$$

We can get the angle in term of z, which includes the motion of C^+ ion. Using the momentum conservation,

$$m_C\, \dot{y'} = 2m_O\, \dot{y}$$
$$m_C\, (\dot{z} - \dot{y}) = 2m_O\, \dot{y}$$
$$\dot{y}\, (2m_O + m_C) = m_c\, \dot{z}$$

$$\tan\theta = \frac{m_C}{(2m_O + m_C)} \frac{\dot{x}}{\dot{z}} \tag{6.19}$$

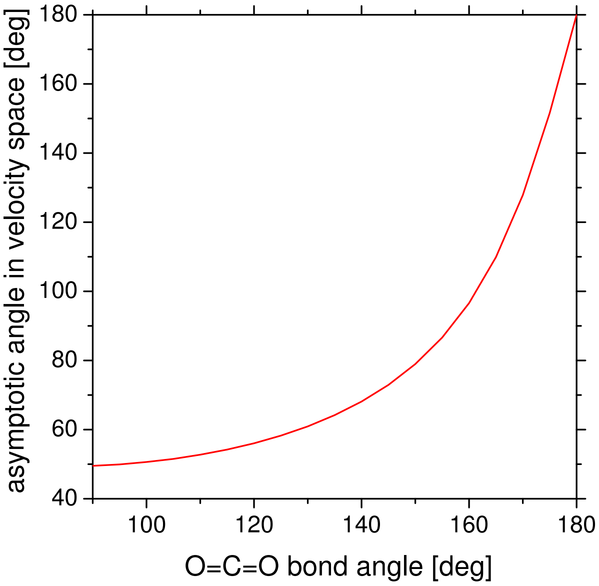

Figure 6.4: Plot between the calculated asymptotic angle between the velocity vector of two O^+ ions and the and initial O=C=O bond angle. These angles are labelled θ and α respectively in the text.

Codes were written in Mathematica to solve equation (6.13 , 6.17) and various parameters such as velocity components ($\dot{x}$, $\dot{y}$), the angle between the velocity vectors can be derived. The calculated asymptotic angle and the initial bond angle are plotted, and shown in Figure 6.4. The relation between the free angle, α and θ is given as

$$\alpha = 2\theta = 2\tan^{-1}\left(\frac{m_C}{(2m_O + m_C)}\frac{\dot{x}}{\dot{z}}\right) \tag{6.20}$$

It is clear from the plot that the trajectory of all fragments are affected by Coulomb repulsion between them. In experimental measurement procedure, it is very difficult to measure the Coulomb effect. Thus, this simulated result gives the mutual relation between the bond angles in lab frame and in molecular frame. As seen in Fig 6.4 the most probable asymptotic angle between the velocity vectors of two O^+ ions is 155°. Based on our simulation, this corresponds to the initial O=C=O bond angle of 168°, implying that triple fragmentation of CO_2^{3+} proceeds from a slightly bent state [Kus09].

6.4 Conclusions

The dissociative geometry of doubly ionized and triply ionized precursor have been mapped by momentum imaging method. The geometry of doubly ionized CH_3Cl is mapped by angular information of each fragments ejected from three-body concerted break-up this ion. We have proposed a simple model to explain the angle between the asymptotic velocity vectors of each fragments. For the observed angular distribution of the fragments our model suggests that the separation of the associative fragment and the heavy residue occurs at distances different from the average separation between the atoms in the neutral molecule. We have found that the geometry CH_3Cl^{2+} precursor is planar instead of deformed tetrahedral.

For mapping the geometry of CO_2^{3+} ion in three-body Coulomb explosion, we have used observed kinematic information of fragments. We have simulated the trajectory of charged fragments ejected in Coulomb explosion and investigated the effect of Coulomb repulsion on its trajectory. We found that the bond angle in momentum space is not same as the actual bond angle. We find that the geometry of CO_2^{3+} is slightly deformed from the linear geometry of the ground state. This is in close agreement with the results of [Sie02] for CO_2^{3+} formed by ion impact.

Chapter 7

Summary and Future Directions

7.1 Summary of the present work

The present work is focused on the study of fragmentation dynamics of polyatomic molecular ions. The molecular ions are created by high energy electron impact on the neutral molecules. The high energy electrons have been chosen to reduce the post collision Coulomb effect on the ionized molecules and thus, the dissociation of molecular ions can be considered a unimolecular process. Some of the singly ionized molecules are metastable but most of the doubly or multiply ionized molecules are unstable. These unstable molecular ions exhibit various processes such as bond dissociation, the atom-atom association, migration of atoms etc. The cross-section for association process is very small compared to the bond dissociation. The interest in the study of association processes in fragmenting polyatomic ion due to possibility of new species formation resulted from atom-atom association or migration of atom and association within molecular ion. We have investigated the migration of atom and bond formation between atoms in the fragmenting molecular ion by ion coincidence momentum imaging technique. Our investigation started from looking at the association reaction in linear (CO_2 and CS_2) and bent (H_2O) triatomic molecules. We found that even in linear molecule the atom-atom association is possible. We have observed the formation of H_2^+ and S_2^+ ions from the dissociative ionization of H_2O and CS_2 molecules respectively. We have found that the probability of observing S_2^+ from CS_2 and H_2^+ ion from H_2O, relative to the simple fragmentation (leading to H^+ or S^+), are roughly equal.

For the study of intra-molecular bond association in polyatomic molecule, the tetrahedral symmetric hydrocarbon CH_4 has been chosen in which all H atoms are geometrically equivalent. Since distortion of the skeletal structure is likely to enhance the association reaction, we compare the associative ion yield from CH_4 with the yield from derivatives of CH_4 which already have a distortion from tetrahedral symmetry. The effect of atom substitution on associative reactions is investigated in CH_3Cl and CH_3OH. In case of CH_4 molecule only formation of H_2^+ ion have been detected but the formation of H_2^+ as well as H_3^+ ions are found from the derivative of methane. The details analysis of these ion formations reveal that the formation of H_2^+ ion formation is roughly the same for CH_3Cl and CH_4. However, there is a large enhancement in case of CH_3OH. In case of triple association (H_3^+ formation), the enhancement due to the presence of –Cl and –OH radicals is pronounced. In fact, the presence of –Cl enhances triple association even more than pair association. This implies that deviation from tetrahedral symmetry in CH_3Cl^{2+} is very large and brings the three H atoms very close to each other. Similar distortion mechanism appears to be present in CH_3OH, but its effect is more favorable for pair association, than triple association.

The role of chemical group in bond association is also investigated in CH_3OH molecule. To distinguish the H atom of hydroxyl group or methyl group, we have used the isotope tagging method. Due to identification of H atom of methyl group and hydroxyl group in CD_3OH molecules the investigation of site-specific atom-atom association have been carried out. The formation of D_2^+, D_3^+ and DH^+, D_2H^+ ion are observed from the singly as well as the doubly ionized CD_3OH molecules. The formation of D_2^+, D_3^+ ions are possible only from the methyl group and the formation of DH^+, D_2H^+ ions are the result of association between D atoms of methyl group and H atom of hydroxyl group. The relative yield analysis is carried out to estimate the contribution of each chemical group in production of these ion. We found that the probability of association of the H atoms on the methyl site alone is nearly four times as large as the probability that the H atom on the hydroxyl site migrates and associates with the H atoms on the methyl site. In CH_3OH also exhibits migration of H atoms, as established by the formation of OH_2^+ from ionized CH_3OH. The formation of OH_2^+ ion is an example of one atom migration and association. In hydrocarbon polyatomic molecule, more than one atom migration and association might be possible.

To investigate the possibility of multi-atom migration and association in polyatomic molecule we have chosen the CH_3CH_2OH molecule and the two structurally very similar molecules acetone (CH_3COCH_3) and dimethyl sulfoxide (CH_3SOCH_3). The evidence of two atom migration have been found in ethanol. We have found the ODH_2^+ ion from dication C_2H_5OD. This ion is an evidence of the migration of two H atoms from the C site of -CH_2- to the hydroxyl -OD site. The formation of this ion is occurred via two-body break-up reaction. Our results indicate that in ethanol, the multi atom migration occurs in the –CH_2OH portion of the molecule and the terminal CH_3– group does not participate.

For more than two atom migration, we have compared the fragmentation pattern of singly and doubly ionized precursor of acetone (CH_3COCH_3) and dimethyl sulfoxide (CH_3SOCH_3). The evidence of more than two atom migration in acetone is not found but in case of sulfoxide, we have detected the signature of three H atom migration. The formation of OH_3^+ in coincidence of CH_3C^+ ion is detected from the analysis of ion-ion coincidence map. The formation of OH_3^+ is possible only when the three H atoms from the methyl group are migrated to O-site before the break-up of precursor. We have done the details momentum map analysis for investigation of break-up pattern of the precursor and formation of this ion. We have found the OH_3^+ ion is ejected in concerted three-body break-up process. Three atom migration in any molecule is a rare process, which requires large structural changes in molecular ion during dissociative ionization. The formation of OH_3^+ ion occurs due to large structural changes in precursor ion. The prediction about the geometrical deformation is difficult due to complex geometrical structure in ground state and possibility of various dissociative state in ionized state. Some of the dissociative state may initiate the multi H atom migration. Mapping of dissociative geometry of precursor may help in understanding the migration and association processes in fragmenting molecular ion.

We have mapped the geometry of molecular ion which dissociate via three-body break-up. Our investigation about the estimation of geometry of precursor is focused only for those three-body reaction which eject the associative product. We have found that the geometry of precursor molecular ion is deformed from the ground state and association takes place during the deformation and before the explosion of ion. Using momentum imaging technique we have successfully mapped the geometry of doubly as well as triply ionized precursor. In case of doubly ionized precursor, we have mapped the geometry of CH_3Cl^{2+}. We have found that the geometry of CH_3Cl^{2+} ion is not deformed tetrahedral but it is planar geometry. We have also mapped the intermediate ion geometry of CH_3OH^{2+} which produces associative ions via sequential or two step process. We have found that the geometry of this precursor which produces various ions such as H_2^+ or HD^+ ion via three distinct reactions have same precursor geometry. In case of triply ionized precursor, we have mapped the geometry of CO_2^{3+} ion. The geometry of this ion is not linear but it is bent. We have done the classical trajectory simulation of all fragments which are ejected from the triply ionized precursor. Simulation is done to estimate the Coulomb effect on the trajectory of fragments. The simulation was necessary to predict the actual geometry of precursor at the time of break-up.

The major conclusions of the work reported here are the following:

1. By comparing the association reactions of bent H_2O and linear CO_2, CS_2, we conclude that the atom association in triatomic molecule depends on the geometry of molecule and perturbation.

2. From the atom association study in polyatomic tetrahedral symmetric molecule (such as CH_4) under high energy (1300 eV) electron impact perturbation, we conclude that the geometrical deformation of this precursor is suitable for pair atom association (formation of H_2^+) but not suitable for triple atom association (formation of H_3^+).

3. The tetrahedral geometry of CH_4 may be deformed if one H atom of CH_4 is substituted by high electronegative atom or radical (such as Cl or OH). The derivative of this molecule such as CH_3Cl has deformed tetrahedral geometry. By comparing the association reactions in CH_4, CH_3Cl and CH_3OH, we found that triple atom association (H_3^+ formation) takes place in the derivatives of CH_4. We conclude that the substitution of electronegative atom in tetrahedral symmetric molecule distorts the geometry of molecule favourably, enhancing the probability of association reactions.

4. From the site specific association study, we conclude that the chemical group (such as methyl or hydroxyl in methanol) contribute differently in association reactions, the chemical group having more H atoms can contribute more in formation H_3^+, H_2^+ ions.

5. From the details study of dissociative ionization of CH_3-SO-CH_3 and CH_3-CO-CH_3molecules, we conclude that the multi atom migration is possible when the electronegative site (such as O) is near to other chemical group (such as –CH_3) having more H atoms.

6. Mapping the geometry of doubly and triply ionized precursor by momentum imaging, we conclude that the geometry of these precursor are deformed from the ground state geometry of parent molecule.

7.2 Future directions

In future, I would like to explore the core shell excitation of atom in polyatomic molecules and its effects on the migration of atom and bond association. Earlier studies [Hay90, Sch08] on the core shell excitation has been established that the core-hole resonance enhances the fragmentation occurring at the core-hole site, while it does not influence the fragmentation far from the core-hole. The influence of this effect on atom association reaction is unexplored. For investigation of these processes, an momentum imaging technique can be used. To study the site-specific fragmentation, we need a intense wide range of photons for perturbation. Synchrotron radiation provides the range of photon energy which can be used in such study.

Mapping of all repulsive excited states of precursor ion which initiate the association reaction is required for understanding the association processes. There may be excited states which can initiate the association reaction, but are dipole forbidden. They may be accessible by multi-photon ionization using an intense laser field, where selection rules no longer hold. Mapping the excited states of molecule using multi-photon ionization is another avenue that may be explored.

Another exciting idea is to investigate the associative reaction channels in a controlled manner. With the availability of femtosecond lasers, controlling the fragmentation reactions is possible. Laser selective chemistry [Zar98, Bri03] and molecular imaging can create a platform for understanding of the interaction of molecules with intense ultrafast laser field. Using these techniques, the molecular vibration or the formation and dissociation of molecules can be observed in real time. By controlling the pulse parameters such as wavelength, the time profile and phase of the excitation pulse, we can try to optimize a wanted reaction channel of dissociating molecular ion and to minimize the unwanted dissociative channels.

Bibliography

[Ait01] D. Aitchison and J. H. D. Eland, Chemical Physics, **263**,(2001) 449–457.

[Amu92] M. Y. Amusia, I.S. Lee and V. A. Kilin, Phys. Rev. A, **45**, (1992) 45764587.

[Bag04] B. Baguenard, J. B. Wills, F. Pagliarulo, F. Lépine, B. Climen, M. Barbaire, C. Clavier, M. A. Lebeault and C. Bordas, Rev. Sci. Instrum., **75**, (2004) 324.

[Bap07] B. Bapat and V. Sharma, J. Phys. B: At. Mol. Opt. Phys., **40**, (2007) 13-19.

[Ben93] I. Ben-Itzhak, K. D. Carnes, S. G. Ginther, D. T. Johnson, P. J. Norris and O. L. Weaver, Phys. Rev. A, **47**, (1993) 3748–3757.

[Ber90] T. Bergmann, T. P. Martin and H. Schaber, Rev. Sci. Instrum., **60**, (1990) 2592.

[Boe82] U. Boesl, H. J. Neusser, R. Weinkauf and E. W. Shlag, J. Phys. Chem., **86**, (1982) 4857.

[Boh13] N. Bohr, Philos. Mag., **26**, (1913) 1–24.

[Bri03] T. Brixner and G. Gerber, Chem. Phys. Chem., **4**, (2003) 418.

[Bry00] W. A. Bryan, J. H. Sanderson, A. El-Zein, W. R. Newell, P. F. Taday and A. J. Langley, J. Phys. B: At. Mol. Opt. Phys., **33**, (2000) 745-766.

[Cha94] F. Chandezon, B. Huber and C. Ristori, Rev. Sci. Instrum., **65**, (1994) 3344–3453.

[Cop94] M. A. Coplan, J. H. Moore and J. P. Doering, Rev. Mod. Phys., **66**, (1994) 985.

[Cor96] C. Cornaggia, Phys. Rev. A, **54**, (1996) 2555–2559.

[Cza07] A. Czasch, J. Milnes, N. Hay, W. Wicking and O. Jagutzki, Nuclear Instruments and Methods in Physics Research Section A: Accelerators, Spectrometers, Detectors and Associated Equipment, **580**, (2007) 1066–1070.

[Daw95] G. Dawber, L. Avaldi, A. G. McConkey, H. Rojas, M. A. MacDonald and G. C. King, J. Phys. B: At. Mol. Phys., **28**, (1995) L271.

[De06] S. De, J. Rajput, A. Roy, P. N. Ghosh and C. P. Safvan, Phys. Rev. Lett. **97** (2006) 213201.

[Dey75] S. Dey, I. E. McCarthy, P. J. O. Teubner and E. Weigold, Phys. Rev. Lett. **34**, (1975) 782–785.

[Dor00] R. Dörner, V. Mergel, O. Jagutzki, L. Spielberger, J. Ullrich, R. Moshammer, H. Schmidt-Böcking, Physics Reports, **330**, (2000) 95–192.

[Dun73] J. L. Duncan, D. C. McKean, P. D. Mallinson, R. D. McCulloch, J. Mol. Spec., **46**,(1973) 232–239.

[Dus23] S. Dushman, Phys. Rev. **21**, (1923) 623.

[Ela91] J. H. D. Eland, Laser Chem., **11**, (1991) 259.

[Fur73] J. B. Furness and I. E. McCarthy, J. Phys. B: Atom. Molec. Phys., **6**, (1973) L204–L207.

[Fur05] Y. Furukawa, K. Hoshina, K. Yamanouchi and H. Nakano, Chem. Phys. Lett., **414**, (2005) 117.

[Gil60] R. J. Gillespie, Canadian J. Chem., **38**, (1960) 818–826.

[Gao84] R. S. Gao, P. S. Gibner, J. H. Newman, K. A. Smith and R. F. Stebbings, Rev. Sci. Instrum., **55**, (1984) 1756.

[Hay90] R. G. Hayes and W. Eberhardt, Phys. Scr., **41**, (1990) 449–453.

[Her66] G. Herzberg, *Electronic spectra and electronic structure of polyatomic molecules*, (1966), Van Nostrand, New York.

[His99] A. Hishikawa, A. Iwamae, and K. Yamanouchi, Phys. Rev. Lett., **83**, (1999) 1127–1130.

[Hue94] A. Huetz, P. Lablanquie, L. Andric, P. Selles and J. Mazeau, J. Phys. B: At. Mol. Phys., **27**, (1994) L13.

[Jag02] O. Jagutzki, J. S. Lapington, L. B. C. Worth, U. Spillman, V. Mergel and H. Schmidt-Böcking, Nuclear Instruments and Methods in Physics Research Section A: Accelerators, Spectrometers, Detectors and Associated Equipment, **477**, (2002) 256–261.

[Kim06] M. H. Kim, B. D. Leskiw, L. S. and A. G. Suits, International Journal of Mass Spectrometry, **252**, (2006) 73–78.

[Kin08] J. S. King, D. S. Price, International Journal of Mass Spectrometry, **277**, (2008) 84–90.

[Kri04] M. Krishnamurthy, F.A. Rajgara, and D. Mathur, J. Chem. Phys. **121**, (2004) 9765.

[Kuc98] K. Kuchitsu (Ed.), *Structure of Free Polyatomic Molecules - Basic Data*, Springer, Berlin, 1998.

[Kus08] R. K. Kushawaha and B. Bapat , Chem. Phys. Lett. **463** (2008) 42-46.

[Kus09] R. K. Kushawaha, S. Sunil Kumar, I. A. Prajapati, K. P. Subramanian and B. Bapat, J. Phys. B: At. Mol. Opt. Phys., **42**, (2009) 105201 (5pp).

[Lap86] J. S. Lapington, H. E. Schwarz, IEEE Transactions on Nuclear Science, **33**, (1986) 288–292.

[Lah91] A. Lahmam-Bennani, J. Phys. B: At. Mol. Phys., **24**, (1991) 2401.

[Lev84] V. G. Levin, V. G. Neudatchin, A. V. Pavlitchenkov and Y. F. Smirnov, J. Phys. B: At. Mol. Phys., **17**, (1984) 1525–1536.

[Lun03] H. Luna, E. G. Cavalcanti, J. Nickles, G. M. Sigaud and E. C. Montenegro, J. Phys. B: At. Mol. Opt. Phys., **36**, (2003) 4717–4729.

[McC91] I.E. McCarthy and E. Weigold, Rep. Prog. Phys., **54**, (1991) 789.

[Mor00] P. Moretto-Capelle, D. Bordenave-Montesquieu and A. Bordenave-Montesquieu, J. Phys. B: At. Mol. Opt. Phys., **33**, (2000) L539–L546.

[Mos96] R. Moshammer, J. Ullrich, M. Unverzagt, W. Schmitt and B. Schmidt-Böcking, Nuclear Instruments and Methods in Physics Research Section B, **108**, (1996) 425–445.

[Nag91] K. Nagesha, B. Bapat, V. R. Marathe and E. Krishnakumar, Chem. Phys. Lett. **230**, (1991) 283–289.

[Par06] B. F. Parsons, S. M. Sheehan, K. E. Kautzman, T. A. Yen and D. M. Neumark, J. Chem. Phys., **125**, (2006) 244301.

[Pos95] J. H. Posthumus, L. J. Frasinski, A .J. Giles and K. Codling, Phys. B. At. Mol. Opt. Phys., **28**, (1995) L349–L353.

[Raj03] F. A. Rajgara, M. Krishnamurthy and D. Mathur, J. Chem. Phys., **119** (2003) 12224.

[Raj06] J. Rajput, S. De, A. Roy and C. P. Safvan, Phys. Rev. A, **74**, (2006) 032701.

[Rei02] E. L. Reichert, G. Thurau and J. C. Weisshaar, J. Chem. Phys., **117**, (2002) 653.

[Ric12] O. W. Richardson, Phil. Mag., **23**, (1912) 594.

[Ren08] X. Ren, A. Dorn, and J. Ullrich, Phys. Rev. Lett., **101** (2008) 093201.

[Roe02] Wim G. Roeterdink and Maurice H. M. Janssen, Phys. Chem. Chem. Phys., **4**, (2002) 601-612.

[Ruh90] E. Ruhl, S. D. Price, S. Leach and J.H.D. Eland, Int. J. Mass Spec. Ion Proc., **97**, (1990) 175.

[Rut09] E. Rutherford, Philos. Mag., **6**, (1909) 21.

[Sai94] N. Saito and I. H. Suzuki, Phys. Scr., **49**, (1994) 80–85

[San99] J. H. Sanderson, T. Nishide, H. Shiromaru, Y. Achiba and N. Kobayashi, Phys. Rev. A, **59**, (1999) 4818–4820.

[Sch08] M. S. Schöffler, J. Titze, N. Petridis, T. Jahnke, K. Cole, L. Ph. H. Schmidt, A. Czasch, D. Akoury, O. Jagutzki, J. B. Williams, N. A. Cherepkov, S. K. Semenov, C. W. McCurdy, T. N. Rescigno, C. L. Cocke, T. Osipov, S. Lee, M. H. Prior, A. Belkacem, A. L. Landers, H. Schmidt-Böcking, T. Weber and R. Dörner, Science, **320**, (2008) 920–923.

[Sch93] O. Schwarzkopf, B. Kr*ä*ssig, J. Elmiger and V. Schmidt, Phys. Rev. Lett., **70**, (1993) 3008.

[Spi01] U. Spillmann, O. Jagutzki, L. Spielberger, R. Dörner, V. Mergel, K. Ullmann-Pfleger and H. Schmidt-Böcking, Phys. Scr., **92**, (2001) 225–226.

[Sch07] M. Schulz, D. Fischer, T. Ferger, R. Moshammer and J. Ullrich, J. Phys. B: At. Mol. Opt. Phys., **40**, (2007) 3091-3099.

[Sha05] V. Sharma and B. Bapat, European Physical Journal D, **37**, (2005) 14–34.

[Sha06] V. Sharma and B. Bapat, J. Chem. Phys. **125**, (2006) 044305.

[Sha07] V. Sharma, Thesis, *Momentum Spectroscopic Studies of Atomic and Molecular Ionisation*, (2007) M. S. University Udaipur, India.

[Shi99] S. Shibata, F. Hirota and T. Shioda, J. of Molec. Stru., **485**(1999) 1-11.

[Sie00] B. Siegmann, U. Werner, R. Mann, N. M. Kabachnik and H. O. Lutz, Phys. Rev. A, **62**, (2000) 022718.

[Sie02] B. Siegmann, U. Werner, H. O. Lutz and R. Mann, J. Phys. B: At. Mol. Opt. Phys., **35**, (2002) 3755-3765.

[Sin06] R. K. Singh, G. S. Lodha, Vandana Sharma, I. A. Prajapati, K. P. Subramanian and B. Bapat, Phys. Rev. A, **74**, (2006) 022708.

[Smy33] H. D. Smyth and D. W. Mueller, Phys. Rev. A, **43**, (1933) 116-120.

[Sta99] H. C. Straub, M. A. Mangan, B. G. Lindsay, K. A. Smith and R. F. Stebbings, Rev. Sci. Instrum., **70**, (1999) 4238.

[Sve74] L.M. Sverdlov, M. A. Kovner and E. P. Krainov, *Vibrational Spectra of Polyatomic Molecules*, (1974) Wiley, New York.

[Tar00] M. Tarisien, L. Adoui, F. Frémont, D. Lelièvre, L. Guillaume, J-Y Chesnel, H. Zhang, A. Dubois, D. Mathur, Sanjay Kumar, M.

Krishnamurthy and A. Cassimi, J. Phys. B: At. Mol. Opt. Phys., **33**, (2000) L11–L20.

[Tri96] L. C. Tribedi, P. Richard, Y. D. Wang, C. D. Lin and R. E. Olson, Phys. Rev. Lett., **77**, (1996) 1996.

[Ull97] J. Ullrich, R. Moshammer, R. Dörner, O. Jagutzki, V. Mergel, H. Schmidt-Böcking and L. Spielberger, J. Phys. B: At. Mol. Opt. Phys., **33**, (1997) 2917–2974.

[Vag89] Z. Vager, R. Naaman and E. P. Kanter, SCIENCE, **244**, (1989) 426–431.

[Wei73] E. Weigold, S. T. Hood and P. J. O. Teubner, Phys. Rev. Lett., **30**, (1973) 475–482.

[Wer03] U. Werner, B. Siegmann, H. Lebius, B. Huber and H. O. Lutz, Nuclear Instruments and Methods in Physics Research Section B, **205**, (2003) 639–642.

[Wil55] W. C. Wiley and I. H. McLaren, Rev. Sci. Instrum., **26**, (1955) 1150.

[Yam06] H. Yamaoka, M. Oura, K. Takahiro, K. Kawatsura, S. Ito, M. Mizumaki, H. Oohashi, Y. Ito and T. Mukoyama, J. Phys. B: At. Mol. Opt. Phys., **39**, (2006) 2747–2756.

[Zar98] R. N. Zare, Science, **279**, (1998) 1875.

[Zha05] K. Zhao and W. T. Hill III, Phys. Rev. A, **71**, (2005) 013412(6).

[Zhe08] M. Zhen-Hua, Z. Bao-Sheng, Z. Xing-Hua and L. Yong-An, Chinese Phys. Lett., **25**, (2008) 2698–2701.

Appendix A

Figures of Merit for the Ion Momentum Spectrometer

The power of our ion momentum spectrometer setup can be seen from its capability to measure the kinematic parameters of charged fragments, as evidenced by the results presented in this thesis. This setup has own figure of merit and hence limitations. We now present the instrumental parameters are mass resolution, momentum resolution, collection efficiency, event rate, etc.

Mass resolution

The mass resolution depends on many parameter as discussed in Chapter 3. The M/$\triangle M$ of present set-up under optimized condition can be obtained for time-of-flight profile of any atomic or molecular system. Here, Ar has taken for this purpose. The FWHM of the Ar^+ time-of-flight profile is 9 ns, while the modal TOF is 7842 ns. This gives a mass resolution M/$\triangle M$ = 436.

Momentum resolution

The limit on the momentum resolution imposed by the spatial resolution of the detector is

$$\triangle p_{x,y} = m \triangle x/t, \quad m \triangle y/t \tag{A.1}$$

where $\triangle p_{x,y}$ is the position resolution of the detector, which is 0.25 mm. For Ar^+, the $\triangle p_{x,y}$ is 2.1 a.u. The detector imposed limit on the p_z resolution is

$$\triangle p_x = qE_s \triangle t \tag{A.2}$$

For 1 ns timing resolution the $\triangle p_z$ comes out to be 0.3 a.u.

These values are purely based on detector and electronic limits. However factor such as molecular beam energy spread, extent of interaction region and field non-uniformity will deteriorate the resolution. The final resolution achieved can be estimated from the width of the distributions of the momentum components of the Ar^+ ion. The value of $\triangle p_{x,y}$ is 14 a.u. and $\triangle p_z$ is 2.4 a.u.

Collection efficiency

The collection efficiency is depends on guided field, kinetic energy of fragments, detector efficiency and so on. Before perform an experiment, we simulate the trajectory of fragments ion which we are interested to detect for a given range of energy. For simulation we used the charged particle trajectory software, TRICOMP. At 60 V/cm guiding field, we have found that the collection efficiency of this setup is 100% for H^+ ion having kinetic energy less than 13 eV irrespective of the direction of emission of the ions.

The detector efficiency is a function of the incident velocity of the particle. In order to achieve a constant efficiency for all ions, ions are often accelerated to an energy of 5 keV. However, in the present setup, we had an acceleration up to 2.8 keV due to instrumentation constraints. This implies an efficiency of about 60 % for light ions and about 40 % for heavy ions, based on generally known MCP characteristics [Gao84, Sta99].

Single collision condition

Most of the experiment have been performed under single collision condition. To archive this, we have used be low electron current (10^8 electron/sec), low molecular beam flux (10^{13} cm^{-3}), very high background vacuum (10^{-7} mbar). The event rate during data acquisition was 100–200 Hz.

Appendix B

Brief description of the CO_2 photo-triple-ionization experiment

The case of photo-triple-ionization of CO_2 was considered to explored the Coulomb repulsion effect on the trajectory of charged fragments ejected from Coulomb explosion of precursor ion. Since triply charged molecular ions could not be formed in the electron-impact experiment, an experiment was performed under photon impact.

The photon source used for this purpose was the Indian Utility Synchrotron (Indus-1), at Raja Ramanna Centre for Advanced Technology, Indore. Indus-1 is a 450 MeV electron storage ring with the radiation flux peaking at 202 eV. Our experiment was performed with 200 eV (6.1 nm) photons. This energy is not resonant with any of the shells of C or O in the CO_2 molecule. It lies between the L and K shell energies of both atoms. Thus the primary process of triple ionization is L electron removal, followed by a combination of CosterKronig and shake-off involving two electrons. No Auger emission is possible at this energy in the C or the O atom.

The photon beam was monochromatized by a toroidal grating monochromator. The monochromatic photon flux ranged between 10^{10} s^{-1} and 10^{11} s^{-1} with energy resolution of 300. A polyamide filter was used to block the second-order diffracted beam from reaching the target. The target was an effusive beam of CO_2 gas. The target gas number density was approximately

10^{12} cm^{-3}, leading to an event rate of about 1.2 kHz. The two beams were orthogonal to each other and to the axis of the ion momentum spectrometer. The overlap volume of the photon beam and the target beam was 1×3 mm^3. The polarization axis was horizontal and parallel to the spectrometer axis. A simple estimate based on the aperture sizes and the spectrometer dimensions puts a geometric lower limit of $\pm 2^\circ$ in the uncertainty of the overlap of the polarization axis with the spectrometer axis. The ion momentum spectrometer was similar as used for electron impact study. Target pressure conditions were also similar, however the photon flux, and hence the ion count rate was higher, at around 500 Hz.

Appendix C

Publications

Papers published

1. Polarisation dependence in non-resonant photo-triple-ionisation of CO_2
   R. K. Kushawaha, S. Sunil Kumar, I. A. Prajapati, K. P. Subramanian and B. Bapat, *J. Phys. B: At. Mol. Opt. Phys.* **42** *105201 (2009)*

2. Fragmentation dynamics of methanol dication
   R. K. Kushawaha and B. Bapat, *Chem. phys. Lett*, **463** 42-46 (2008).

3. Breakup of SF_6^{3+} photoion revealed by momentum correlation between fragments
   S. Sunil Kumar, P. C. Deshmukh, **R. K. Kushawaha**, V. Sharma, I. A. Prajapati, K. P. Subramanian, and B. Bapat,*Phys. Rev. A* **78** 062706 (2008).

Papers under preparation

1. Signatures of functional group dependence in kinetic energy distributions of H_2^+ and H_3^+ ions from methanol
   R. K. Kushawaha and B. Bapat.

2. Bond association dynamics in dissociation of CH_3Cl^{2+}
   R. K. Kushawaha and B. Bapat.

3. Momentum correlation in many-body explosion of SF_6 under ion impact
   R. K. Kushawaha, M. R. Jana, C. P. Safvan, S. Sunil Kumar, I. A. Prajapati and B. Bapat.

Acknowledgements

A large group of people has contributed to this thesis, and without their great support in various ways, it would simply not have been possible to perform the experiment, analyze the data, and understand the results as presented in thesis.

First and foremost, I express my gratitude to my thesis advisor Dr. Bhas Bapat for his continuous support, scientific guidance and many inspiring discussions throughout the Ph.D. program. He was always there to listen and to give advice. This thesis grew out of a series of dialogues with him. He showed me different ways to approach a research problem and the need to be persistent to accomplish any goal. In the beginning of my research, understanding the depth of the research problems was very difficult and most of the problems seemed to be unsolvable or experimentally difficult to tackle within Ph.D. tenure. Whenever I fell in such a situation, I usually contacted Bhas sir and discussed my views. He smartly gave answers to my questions and also at the end of the discussions made me understand the depth and many phases of the problem. His enthusiasm and words of motivation have always inspired me and helped me to do better each time. He gave me the freedom to pursue my research interests.

I must acknowledge the invaluable contributions of Dr K P Subramanian. Without discussion with him, my understanding in this field would have been superficial at best. I have gained a lot by discussion with him, to whom I am much obliged for his encouraging comments which gave me a right path of academic and personal improvement.

During my tenure we have performed experiments at Centre for Advance Technology (CAT), Indore in collaboration with Prof P C Deshmukh group of Indian institute of Technology Madras, Chennai. This was the first experience in performing experiments in collaboration. The experiments could not have been possible without the help of the staff at CAT. I am grateful to all of them, specially to Prof G S Lodha for full support and encouragement. I would like to express my gratitude to Prof P C Deshmukh and S Sunil Kumar of IIT Madras for support and encouragement to investigate the properties of molecules by synchrotron radiation.

We have also performed experiments at Inter-University Accelerator Centre (IUAC), Delhi. The experiments are successful due to the help of the staff at IUAC. I am grateful to all of them, specially to Prof A Roy, Dr C P Safvan, Dr Sankar De, Dr Jyoti Rajput and Mridula Rani Jana.

I thank Prof U Sarkar, Prof R Ramesh, Prof S Mohanty, Prof S Ramachandran, Prof D P K Banerjee and all other members of academic committee for critically reviewing the progress of my work and giving valuable suggestions at various stages of my research.

I am deeply indebted to our Director, Prof J N Goswami for magnanimous support. His encouraging remarks during one of his talks, about designing ones own apparatus, gave me strength to pursue research using an experimental setup designed in PRL. My warm thanks go to our Dean, Prof. A. K. Singhvi. I will never forget his kind help, cooperation and support whenever I needed it.

I acknowledge Prof Prasanta K Panigrahi, Dr Angom Dilip Kumar Singh for discussion and suggestions about possible theoretical work in molecular physics. I thank Dr Namit Mahajan for his help in formulation of the study of Coulomb explosion of multiply charged molecular ions. A special thanks goes to Santosh K Singh for helping the Mathematica programming in one of my research problem.

I sincerely thank colleagues in the group, I A Prajapati, S B Banerjee and V K Lodha, for their continuous assistance in the setting up of my experimental apparatus and for their constructive criticism and encouragement. I learned basics of electronics from our past senior group member A P Gohil, I would like to acknowledge him for his teaching and encouragement. I learned about the MCP detector from Dr Rajesh K Singh. I would like to thank him for his teaching, support and encouragement.

I am deeply indebted to all other members of Space and Atmospheric Sciences division for their constant encouragement through thoughts and ideas. I specially acknowledge Prof R Sekar, Prof Shyam Lal, Prof A Jayaraman, Prof S A Haider, Prof S Ramachandran, Dr Varun Sheel, and Dr D Pallamraju.

I am deeply indebted to my senior colleagues and friends, Dr Vandana Sharma and Dr Rahul C Purandare, who have been an inspiration on how to gain perfection in work. A special acknowledgement goes to them for many years of help and meaningful discussions.

I would like to express my gratitude to other colleagues in my laboratory Arvind Kumar Saxena, Amrendra Pandey, and Koushik Saha, for fruitful discussions and various insights and also have been supportive in every way. I extend my gratitude to my other colleagues Dibyendu Chakrabarty, Som Kumar Sharma, Amit Mishra, Shilpy Gupta, Shuchita Srivastava, Sumita Kedia, Sumanta Sarkhel, Iman Guha, Rohit Srivastava, Sanat K Das and Uma Das. A special thank and acknowledgement goes to Bhavesh G. Patel for helping the MatLab programming and encouragement.

I would like to express my gratitude to my batchmates Ritesh, Salman, Rohit, Santosh, Akhilesh, Ramkrishna and Nabi for their nice company.

I also acknowledge with thanks the generous support of the staff of the mechanical workshop, library, maintenance, liquid nitrogen plant, computer centre and accounts section. Special thanks are due to P Ubale, H R Vaghela, Jigar Raval, G G Dholakia, Hitendra Mishra, Alok Shrivastava, Siva, Nishtha, Uma Desai, Parul Parikh, Jaishree, A Puthawala and A K Jain and all others for their help.

My health was fully dependent on the food provided by the hostel canteen and PRL's canteen. I was fit and gained almost 10 kg weight during Ph.D. tenure. A great thank-you goes to all the staff members of the canteen and the hostel who have taken care of daily needs.

I would like to express my gratitude to my TV room partners Gyana, Alok, Avasthi and Navin Chauhan for creating a full entertainment environment.

Well, I was not a good volleyball player but I enjoyed playing volleyball at PRL quatrangle during my PhD tenure. I thank Arvind Singh, Amjad, Rabiul, Vinit, Arvind purohit, Jha ji, Vimal, Pankaj, Waliur Rahman, Brajesh Kumar Mani, Soumya Rao, Ashwini, Suman Acharyya, Sandeep Gautam, Ashok, Shreekant, Patra, S Sarkhel, Bhasvar, Lokesh K Dewangan and all other volleyball players who created sporting environment in PRL residence. I extend my gratitude to Bhavik Kodrani, Vishal H Joshi, Shreyas Managave, Shasdhar, Harinder, Manan and Suratna Das for their nice company, support and encouragement.

This work would not have been possible without the blessings of my parents. They allowed me total freedom to pursue my dreams, and were always there for moral support. Words cannot express my gratitude towards them. Special thanks go to Nisha Kushawaha for moral support, caring and encouragement. Words of encouragement from my brothers Brijesh K Kushawaha and Premprakash Kushawaha, and my sisters Chanda and Tara have always helped me in beating the challenges of my Ph.D. life.

Rajesh Kumar Kushawaha